The SWI/SNF chromatin remodeling assemblies BAF and PBAF differentially regulate cell cycle exit and cellular invasion *in vivo*

Jayson J. Smith[1], Yutong Xiao[1], Nithin Parsan[2], Michael A. Q. Martinez[1], Frances E. Q. Moore[1], Nicholas J. Palmisano[1], Abraham Q. Kohrman[3], Mana Chandhok Delos Reyes[4], Rebecca C. Adikes[1], Taylor N. Medwig-Kinney[1], Simeiyun Liu[1,5], Sydney A. Bracht[1,6], Wan Zhang[1], Kailong Wen[7,8], Paschalis Kratsios[7,8], David Q. Matus[1,9]

[1]Department of Biochemistry and Cell Biology, Stony Brook University, Stony Brook, NY 11794, USA

[2]Massachusetts Institute of Technology, Cambridge, MA 02139, USA

[3]Department of Molecular Biology, Princeton University, Princeton, NJ 08544, USA

[4]10 Grant St., Somerville, MA 02145, USA

[5]Department of Biology, Stanford University, Stanford, CA 94305, USA

[6]Department of Cell Biology, Johns Hopkins University, Baltimore, MD 21205, USA

[7]The Grossman Institute for Neuroscience, Quantitative Biology, and Human Behavior, University of Chicago, Chicago, IL 60637, USA

[8]Department of Neurobiology, University of Chicago, Chicago, IL 60637, USA

[9]Lead Contact

[*]Correspondence: david.matus@stonybrook.edu

SUMMARY STATEMENT

Cellular invasion through basement membranes by the *C. elegans* anchor cell requires both BAF- and PBAF SWI/SNF complexes to arrest the cell cycle and promote the expression of pro-invasive genes.

SUMMARY

Chromatin remodeling complexes, such as the SWItching defective/Sucrose Non-Fermenting (SWI/SNF) ATP-dependent chromatin remodeling complex, coordinate metazoan development through broad regulation of chromatin accessibility and transcription, ensuring normal cell cycle control and cellular differentiation in a lineage-specific and temporally restricted manner. Mutations in subunits of chromatin regulating factors are associated with a variety of diseases and cancer metastasis co-opts cellular invasion found in healthy cells during development. Here we utilize *Caenorhabditis elegans* anchor cell (AC) invasion as an *in* vivo model to identify the suite of chromatin and chromatin regulating factors (CRFs) that promote cellular invasiveness. We demonstrate that the SWI/SNF ATP-dependent chromatin remodeling complex is a critical regulator of AC invasion, with pleiotropic effects on both G_0/G_1 cell cycle arrest and activation of invasive machinery. Using targeted protein degradation and RNA interference (RNAi), we show that SWI/SNF contributes to AC invasion in a dose-dependent fashion, with lower levels of activity in the AC corresponding to aberrant cell cycle entry and increased loss of invasion. Finally, we implicate the SWI/SNF BAF assembly in the regulation of the cell cycle, whereas our data suggests that the SWI/SNF PBAF assembly promotes AC attachment to the basement membrane (BM)

and promotes the activation of the invasive machinery. Together these findings demonstrate that the SWI/SNF complex is necessary for two essential components of AC invasion: arresting cell cycle progression and remodeling the BM. The work here provides valuable single-cell mechanistic insight into the contributions of SWI/SNF assembly and subunit-specific disruptions to tumorigenesis and cancer metastasis.

Keywords: Chromatin regulating factors, chromatin remodeling, SWI/SNF, BAF, PBAF, cell invasion, cell cycle exit, *C. elegans*

INTRODUCTION

Cellular invasion through BMs is a critical step in metazoan development and fitness. Early in hominid development, trophoblasts must invade into the maternal endometrium for proper blastocyst implantation (1). In the context of immunity, leukocytes become invasive upon injury or infection to travel between the bloodstream and interstitial tissues (2,3). Atypical activation of invasive behavior is associated with a variety of diseases, including rheumatoid arthritis wherein fibroblast-like synoviocytes adopt invasive cellular behavior leading to the expansion of arthritic damage to previously unaffected joints (4,5). In addition, aberrant activation of cell invasion is one of the hallmarks of cancer metastasis (6). A variety of *in vitro* and *in vivo* models have been developed to study the process of cellular invasion at the genetic and cellular levels. *In vitro* invasion assays typically involve 3D hydrogel lattices, such as Matrigel, through which cultured metastatic cancer cells will invade in response to chemo-attractants (7). Recently, microfluidic systems have been integrated with collagen matrices to improve these *in vitro* investigations of cellular invasion (8). While *in vitro* invasion models provide an efficient means to study the mechanical aspects of cellular invasion, they are currently unable to replicate the complex microenvironment in which cells must invade during animal development and disease.

A variety of *in vivo* invasion models have been studied, including cancer xenograft models in mouse (9–11) and zebrafish (12,13), which each have their respective benefits and drawbacks. Over the past ~15 years, *Caenorhabditis elegans* anchor cell (AC) invasion has emerged as a unique alternative model due to the visually tractable single-cell nature of its cell invasion (**Fig 1A**) (14). Previous work has

demonstrated a high degree of evolutionary conservation in the cell-autonomous mechanisms underlying BM invasion (3,15), including basolateral polarization of the F-actin cytoskeleton and cytoskeletal regulators and the expression of matrix metalloproteinases (MMPs) (16–21). We have also previously demonstrated that the AC requires the expression of transcription factors (TFs) common to metastatic cancers, including *egl-43* (EVI1/MEL), *fos*-1 (FOS), *hlh-2* (E/Daughterless), and *nhr-67* (TLX/Tailless) in order to breach the BM (22) (**Fig 1 B**). In addition to the expression of pro-invasive genes, there is increasing evidence that cells must also arrest in the cell cycle to adopt invasive behavior (23). Our previous work has demonstrated that the AC must terminally differentiate and arrest in the G_0/G_1 phase of the cell cycle to invade the BM and make contact with the underlying primary vulval precursor cells (1° VPCs) (22,24). The specific cell cycle regulatory mechanisms that govern differentiation and cell cycle arrest in the AC and the connection between G_0/G_1 arrest and cellular invasion have yet to be resolved.

The decision to maintain a plastic cell fate or to undergo cell fate specification and terminal differentiation is in part the consequence of a complex, genome-wide antagonism between Polycomb group (PcG) transcriptional repression and Trithorax group (TrxG) transcriptional activation (25–27). For example, the binding of pioneer transcription factors OCT4 and SOX2 to target DNA in order to retain pluripotency in murine embryonic stem cells is the indirect consequence of the regulation of chromatin accessibility at these target regions (28). A recent study has shown that chromatin accessibility of enhancers in crucial cell cycle genes which promote the G_1/S transition, including Cyclin E and E2F transcription factor 1, is developmentally restricted to

reinforce terminal differentiation and cell cycle exit during *Drosophila melanogaster* pupal wing morphogenesis (29). In *C. elegans* myogenesis, the SWItching defective/Sucrose Non-Fermenting (SWI/SNF) ATP-dependent chromatin remodeling complex, a member of the TrXG family of complexes, both regulates the expression of the MyoD transcription factor (*hlh-1*) and acts redundantly to promote differentiation and G_0 cell cycle arrest with core cell cycle regulators: cullin 1 (CUL1/*cul-1)*, cyclin-dependent kinase inhibitor 1 (*cki-1)*, FZR1 (*fzr*-1), and the RB transcriptional corepressor (RBL1/*lin*-35). The importance of chromatin regulating factors (CRFs) for the acquisition and implementation of differentiated behaviors is also reflected in the AC, as previous work has shown that the histone deacetylase *hda-1* (HDAC1/2) is required for pro-invasive gene expression and therefore differentiated cellular behavior and invasion into the underlying BM (24) (**Fig 1 B**). Given these findings, a comprehensive investigation of the regulatory mechanism governing AC invasion should include a thorough description of the suite of CRFs required for G_0/G_1 cell cycle arrest and invasive differentiation in the AC.

In this study we perform an RNA interference (RNAi) screen of *C. elegans* CRFs, specifically focusing on genes involved in chromatin remodeling complexes or histone modification. We identify 41 genes which are crucial for cellular invasion. Among the CRFs identified as significant regulators of AC invasion, the SWI/SNF complex emerged as the most well-represented single chromatin remodeling complex. RNAi knockdown of subunits specific to the SWI/SNF core (*swsn-1* and *snfc-5/swsn-5*), and both BAF (BRG/BRM-Associated Factors; *swsn-8/let-526*) and PBAF (Polybromo Associated BAF; *pbrm-1* and *swsn-7*) assemblies resulted in penetrant loss of AC invasion. We

generated fluorescent reporter knock-in alleles of subunits of the core (*swsn-4::GFP*) and BAF (*swsn-8::GFP*) assemblies of the SWI/SNF complex using CRISPR/Cas9-mediated genome engineering. These constructs, used in conjunction with an endogenously labeled PBAF (*pbrm-1::eGFP*) assembly, enabled us to both determine the developmental dynamics of the complex core and assemblies, and to gauge the efficiency of various knockdown strategies. Using newly generated RNAi constructs and an anti-GFP nanobody, we demonstrated that the cell autonomous contribution of the SWI/SNF complex to AC invasion is dose-dependent. This finding parallels similar studies in cancer (30–33) and *C. elegans* mesoblast development (34). Examination using a DNA Helicase B (DHB)-based CDK activity sensor (35) revealed assembly-specific contributions to AC invasion: whereas BAF promotes AC invasion in a cell cycle-dependent manner, PBAF contributes to invasion in a cell cycle-independent manner. Finally, we utilized the auxin-inducible degron (AID) system combined with PBAF RNAi to achieve strong PBAF subunit depletion in the AC, which resulted in loss of both AC invasion and adhesion to the BM. Together, these findings provide insight into how the SWI/SNF complex assemblies may contribute to distinct aspects of proliferation and metastasis in human malignancies.

RESULTS

An RNAi screen of 270 chromatin regulating factors identified the SWI/SNF complex as a key regulator of AC invasion

We generated an RNAi sub-library of 270 RNAi clones from the complete Vidal and Ahringer RNAi libraries (36,37) targeting genes implicated in chromatin state, chromatin remodeling, or histone modification (**Table S1**) to identify the suite of CRFs

that, along with *hda-1*, contribute to AC invasion (**Fig 1 B**). Because CRFs act globally to control gene expression, we screened each RNAi clone by high-resolution DIC and epifluorescence microscopy in a uterine-specific RNAi hypersensitive background containing labeled BM (*laminin::GFP*) and an AC reporter (*cdh-3>PH::mCherry*) (**Fig 1 A; Table S1**) (14,22,24,38). This genetic background allowed us to limit the effect of transcriptional knockdown of CRFs to only affect the AC and the neighboring uterine tissue, and only for a time period following the specification of the AC (38). RNAi-mediated knockdown of the majority of CRF genes (227/270 genes, 84%) resulted in defects in AC invasion (**Table S1**), suggesting a general requirement for chromatin regulation in cellular invasion. For ease of study, we chose to verify the 41 genes whose RNAi clones resulted in penetrant AC invasion defects (AC invasion defect >20%, n≥30 animals), as indicated by a failure to breach the BM by the time wild-type ACs have normally invaded and contacted the grand-daughters of the 1˚ fated P6.p vulval precursor cell (P6.p 4-cell stage; **Table S2**). Five subunits of the SWI/SNF ATP-dependent chromatin remodeling complex were recovered as significant regulators of AC invasion: *swsn-1*(SMARCC1/SMARCC2; 23% AC invasion defect), *swsn-5/snfc-5* (SMARCB1; 20% AC invasion defect), *swsn-7* (ARID2; 23% AC invasion defect), *swsn-8*/*let-526* (ARID1A/ARID1B; 23% AC invasion defect), and *pbrm-1* (PBRM1; 20% AC invasion defect) (**Table S2**). As such, the SWI/SNF complex is the most well-represented single chromatin remodeling complex detected in our screen, with representation of the core (*swsn-1*, *swsn-5/snfc-5*), BAF (*swsn-8*) and PBAF (*pbrm-1* and *swsn-7*) assemblies. Given the prevalence of SWI/SNF subunits in our CRF RNAi screen and the crucial role SWI/SNF plays in the regulation of animal development (39–

44), tumorigenesis (31,45–47), and cell cycle control (34,48–51), we chose to focus our efforts on characterizing the role of the SWI/SNF complex in promoting AC invasion.

To confirm our RNAi results implicating the SWI/SNF complex in the promotion of AC invasion, we obtained two temperature sensitive hypomorphic alleles, *swsn-1(os22)* and *swsn-4(os13)* (40), and scored for defects in AC invasion in a genetic background containing both BM (*laminin::GFP*) and AC (*cdh-3>mCherry::moeABD*) reporters. While we observed no defects in AC invasion in animals grown at the permissive temperature (15°C) (**Fig S1 A**), animals containing hypomorphic alleles for core subunits *swsn-1* and *swsn-4* cultured at the restrictive temperature (25°C) displayed defects in 20% (10/50) and 24% (12/50) of animals, respectively, corroborating our RNAi results and further supporting the necessity of SWI/SNF chromatin remodeling for AC invasion (**Fig S1 B**).

Improved RNAi vectors revealed distinct contributions of SWI/SNF subunits to AC invasion

BAF and PBAF are the two primary SWI/SNF assemblies in *C. elegans* (**Fig 2 A**). Both assemblies are composed of common factors, including an ATPase-containing core (*swsn-1, swsn-4, swsn-5/snfc-5*) and accessory subunits (*swsn-2.1/ham-3, swsn-2.2, swsn-3, swsn-6,* and *phf-10*) (45,52). These common factors are bound by assembly-specific subunits in a mutually exclusive manner, which confers the distinct character of each of the two assemblies. In *C. elegans,* either SWSN-8 and DPFF-1 proteins associate with common factors to form the BAF assembly, or PBRM-1, SWSN-7, and SWSN-9 associate with common factors to form the PBAF assembly (42,53,54). Prior investigations into SWI/SNF have revealed a wide array of developmental contexts

in which the BAF and PBAF complexes have overlapping and distinct roles in the regulation of cell cycle control, differentiation, and differentiated behavior (34,48,54–59).

First, we generated improved RNAi constructs utilizing the T444T vector targeting representative subunits of the core and both SWI/SNF assemblies to investigate the contribution of individual SWI/SNF subunits to AC invasion and to distinguish the potentially distinct roles of the BAF and PBAF assemblies in the regulation of this process (60) (**Table S3**). Knockdown of SWI/SNF subunits in the AC following treatment with T444T RNAi vectors resulted in penetrant loss of invasion. The majority of ACs failed to invade in whole-body RNAi sensitive animals treated with RNAi targeting the core SWI/SNF ATPase (*swsn-4*) or core component *swsn-1* (90% and 94%, respectively; n=50 animals; **Fig 2 B, E**). RNAi-mediated loss of the BAF assembly (*swsn-8*) also displayed a significant loss of AC invasion (32%; n=50 animals; **Fig 2 C, E**). Knockdown of the PBAF assembly subunits in the AC with *pbrm-1(RNAi), swsn-7(RNAi)*, or *swsn-9(RNAi)* resulted in a less penetrant loss of AC invasion (18%, 20%, and 12%, respectively; n=50 animals; **Fig 2 D, E**). Interestingly, RNAi-mediated knockdown of *swsn-1*, *swsn-4* or *swsn-8* also resulted in multiple uterine cells expressing the *cdh-3>mCherry::moeABD* AC reporter which failed to invade the BM (*laminin::GFP*) (32%, 30% and 8%, respectively; **Fig 2 B-C, E**). In all instances where more than one cell expressed the AC specification marker, no breach in the underlying BM was detected at the P6.p 4-cell stage. In contrast, only single non-invasive ACs were evident following RNAi treatment targeting PBAF assembly subunits (**Fig 2 D-E**). These results suggest that the SWI/SNF assemblies may promote AC invasion through regulation of both a cell cycle-dependent and -independent mechanism.

Characterization of endogenous GFP-tagged alleles and the efficacy of improved SWI/SNF RNAi vectors

Next, to confirm expression of SWI/SNF subunits in the AC and to assess the potency of our SWI/SNF RNAi vectors we utilized CRISPR/Cas9 genome engineering to generate GFP-tagged alleles of *swsn-4* and *swsn-8*, inserting a codon-optimized GFP tag into the 5' end and 3' end of the *swsn-4* and *swsn*-8 loci, respectively (**Fig S2 A**) (61). We also obtained a strain containing an endogenously eGFP-labeled PBAF subunit *pbrm-1::eGFP*. The GFP-tagged endogenous strains showed ubiquitous *SWSN-4::GFP, SWSN-8::GFP,* and *PBRM-1::eGFP* nuclear localization throughout the *C. elegans* developmental life cycle (**Fig S2 B**). We quantified fluorescence expression of SWI/SNF core ATPase (SWSN-4::GFP), BAF (SWSN-8::GFP), and PBAF (PBRM-1::eGFP) in the AC during vulval development across the L3 and early L4 stages, as defined by the division pattern of the 1°-fated VPC (14) (n≥30 animals per stage; **Fig S3 A-C'**). Expression of all three subunits was enhanced in the AC relative to the neighboring ventral uterine (VU; *swsn-4*: 18%, *swsn-8*: 21%, *pbrm-1*: 17% enhanced) and 1° VPC (*swsn-4*: 30%, *swsn-8*: 38%, *pbrm-1*: 23% enhanced) lineages during AC invasion (**Fig S3 A'-C'**). Late in vulval development at the P6.p 8 cell stage, expression of *swsn-4::GFP* and *pbrm-1::eGFP* increases in the 1° VPCs and is no longer statistically separable from expression in the AC, whereas expression of SWSN-8::GFP in the VPCs remains significantly lower than in the AC (**Fig S3 A'-C'**).

We treated SWI/SNF endogenously labeled GFP-tagged strains with our RNAi vectors to precisely quantify the efficiency of RNAi-mediated loss of expression of target

SWI/SNF complex subunits and to correlate this loss with the resulting AC phenotypes. Treatment with either *swsn-4(RNAi)* or *swsn-8(RNAi)* vectors resulted in robust depletion of fluorescence expression of SWSN-4::GFP (94% depletion) and SWSN-8::GFP (81% depletion) in the AC (**Fig S4 A-B, D**) and penetrant loss of invasion (90% and 30%, respectively; n=30 animals for each condition; **Fig S4 E**). We also noted instances where multiple cells expressed the AC reporter (23% and 10%, respectively; n=30 animals for each condition; **Fig S4 E**). Treatment of the PBRM-1::eGFP strain with *pbrm-1(RNAi)* vector revealed significant knockdown of PBRM-1 protein (49% depletion), but a low penetrance of invasion defects (17%; n=30 animals; **Fig S4 C-E**). Altogether, these results confirmed the differential expression of SWI/SNF core, BAF, and PBAF subunits in the AC and demonstrated the effectiveness of our improved SWI/SNF-targeting RNAi vectors.

The SWI/SNF ATPase SWSN-4 provides dose-dependent regulation of AC invasion

The degree to which the SWI/SNF complex contributes to tumorigenesis in clinical settings has been linked to the dose of functional SWI/SNF ATPase in precancerous and transformed cells (31,33,62). Previous work in *C. elegans* has demonstrated a similar dose-dependent relationship between SWI/SNF and cell cycle control (34). We modulated expression of SWSN-4::GFP using a combination of RNAi-mediated knockdown and AC specific GFP-targeting nanobody technology to determine whether the phenotypic dosage-sensitivity seen in cancer and *C. elegans* mesodermal

(M) cell development is also characteristic of SWI/SNF in the promotion of AC invasion (63).

Though RNAi treatment targeting SWI/SNF components in endogenous strains resulted in significant knockdown of fluorescence expression of SWSN-4::GFP in the AC, loss of expression was noted in many other tissues in treated animals, including the 1° VPCs, which contribute to AC invasion non-autonomously (14,64) (**Fig S4**). We used an anti-GFP nanobody to achieve lineage-restricted protein depletion and limit loss of expression to the AC (63) (**Fig 3**). We generated two anti-GFP nanobody constructs, using conserved *cis*-regulatory elements from the *cdh-3* and *egl-43* promoters (22,24,38,65,66) and introduced them to a strain containing an endogenous GFP-tagged allele of *swsn-4* as well as background AC and BM reporters (**Fig 3 B-C**). The *cdh-3*-driven anti-GFP nanobody resulted in a weak reduction of SWSN-4::GFP levels with no significant difference in fluorescence expression in the AC compared to wildtype animals (5.6% depletion; n=80 animals; **Fig 3 F**). However, it expressed specifically in the AC and resulted in defective AC invasion, suggesting partial loss of function (21% AC invasion defect; n=102; **Fig 3 B, G**). In contrast, the *egl-43>antiGFP-nanobody* expressed highly in the AC but also in the neighboring ventral and dorsal uterine (VU/DU) cells (**Fig 3 C**, asterisk) (22,38,65). As the AC invades independently of VU/DU cells (14), anti-GFP expression in these tissues should not affect AC invasion. Similar to animals treated with *swsn-4(RNAi)* (**Fig 3 D**), *egl-43>antiGFP-nanobody*-mediated protein depletion of SWSN-4::GFP resulted in a significant loss of fluorescence expression in the AC (70% GFP depletion; n=80 animals; **Fig 3 C, F**) as well as a penetrant loss of invasion and a low frequency of animals with multiple cells expressing

the AC specification marker (88.2% AC invasion defect, 2.5% multiple AC phenotype; n=101 animals; **Fig 3 G**).

In an effort to further deplete *swsn-4* expression in the AC, we fed transgenic *egl-43>antiGFP-nanobody* animals *swsn-4* RNAi (**Fig 3 E**). Strikingly, in this combination knockdown strategy, 100% of AC invasion was lost and the frequency of multiple cells expressing the AC specification reporter drastically increased relative to treatment with *swsn-4(RNAi)* or the *egl-43*-driven anti-GFP nanobody conditions alone (83%; n=41 animals; **Fig 3 G**). Though the combination of RNAi and anti-GFP depletion resulted in strong loss of expression of the core ATPase of the SWI/SNF complex, the fluorescence expression was not significantly different relative to treatment of the *swsn-4::GFP* endogenous strain with *swsn-4* RNAi alone (92.6% and 91.6% GFP depletion, respectively; n≥45 animals for each treatment; **Fig 3 G**). Our reasoning is that this is likely due to measurement of fluorescence values which are beyond our threshold ability to quantify based on the fluorescence detection limits of our imaging system.

A recent study focusing on cell cycle control of SWI/SNF throughout *C. elegans* muscle and epithelial differentiation demonstrated tissue and lineage-specific phenotypes following weak or strong loss of core SWI/SNF subunits (32). Within the M lineage that gives rise to posterior body wall muscles (BWMs), coelomocytes (CCs), and reproductive muscles or sex myoblast (SMs) descendants, different cell types responded differently to loss of SWI/SNF. In the BWM, strong loss of SWI/SNF resulted in hyperproliferation, similar to the phenotype we detect in the AC. The opposite is true in the SM lineage, where modest knockdown of *swsn-4* resulted in hyperproliferation while complete loss of *swsn-4* expression resulted in a null phenotype where SMs

failed to divide and arrest in S phase (34). Thus, we next sought to determine whether the hyperproliferation phenotype we detected in the AC by improved RNAi was indicative of a *swsn-4* null phenotype. To determine this, we treated animals containing a lineage-restricted CDK activity sensor (*unc-62>DHB::2xmKate2*) with *swsn-4(RNAi)* (**Fig S5 A**). We then determined the number (**Fig S5 B**) and cell cycle state (**Fig S5 C**) of SM cells at a time when the majority of SMs in control animals had finished cycling and subsequently differentiated (late P6.p 8 cell stage; 16 SM cell stage). Animals treated with *swsn-4(RNAi)* had significantly fewer SM cells than controls (mean SMs/animals = 5; n=31 animals; **Fig S5 B**) with many instances of SMs that failed to enter a single round of cell division (n=20 single SMs out of 43 animals). Interestingly, 27.9% (12/43) of animals treated with *swsn-4(RNAi)* were absent of SMs on either the left or the right side, whereas 100% (30/30) control animals had SMs on both sides, which may indicate a defect in either specification or migration of SMs (**Fig S5 B**). We then employed a cyclin-dependent kinase (CDK) sensor, which uses a fragment of mammalian DNA Helicase B (DHB) fused to two copies of mKate2 (35,67), to quantify cell cycle state. In cells with low CDK activity that are quiescent or post-mitotic, the ratiometric CDK sensor is strongly nuclear localized (35,66,67). In cycling cells with increasing CDK activity, the CDK sensor progressively translocates from the nucleus to the cytosoplasm, with a ratio approaching 1.0 in S phase and >1 in cells in G_2 (35). Thus, the cytoplasmic:nuclear (C/N) ratio of DHB::2xmKate2 can serve as a proxy to identify cell cycle state. Quantification of the cell cycle state in single SMs that fail to ever divide in the *swsn-4(RNAi)* condition resulted in a mean C/N ratio indicative of arrest in S phase (35) (Avg. C/N ratio = 0.803; n=20 SMs; **Fig S5 C**), whereas SMs in

the control condition are differentiating and arrest in a G_0 cell cycle state (mean C/N ratio=0.320; n=90 SMs; **Fig S5 C**). These results demonstrated that the improved *swsn-4* RNAi targeting vector phenocopied the *swsn-4* null condition in the SM lineage, as we detected both the hypoproliferative phenotype and S-phase arrest that was observed using a lineage-restricted catalytically inactive SWI/SNF ATPase (34). Altogether, our data demonstrated that in the AC, the SWSN-4 core ATPase of the SWI/SNF complex contributes to invasion in a dose-dependent manner: moderate loss of expression produced non-invasive single ACs while extreme loss of expression led to a non-invasive hyperproliferative state.

The BAF assembly contributes to AC invasion via regulation of cell cycle arrest

Having established that strong depletion of the SWI/SNF complex results in a fully penetrant defect in AC invasion with a high percentage of animals possessing multiple, non-invasive ACs (**Fig 3**), we next sought to determine whether the extra ACs observed were the result of inappropriate AC proliferation (22,66). To determine whether the SWI/SNF complex is required for G_0/G_1 cell cycle arrest in the AC, we quantified AC CDK activity using a ubiquitously expressed *rps-27*>DHB::GFP transgene paired with an AC-specific reporter (*cdh-3>mCherry::moeABD*) in live animals following RNAi-mediated knockdown of SWI/SNF core (*swsn-4*), BAF (*swsn-8*), and PBAF (*pbrm-1*) subunits (**Fig 4**). In wild-type invasive ACs, we observed strong nuclear localization of the CDK sensor and quantified a cytoplasmic/nuclear (C/N) ratio indicative of G_0 arrest (mean C/N: 0.226, n=68 animals) (**Fig 4 A, E**). In animals treated with *pbrm-1(RNAi)*, the CDK sensor also localized principally in the nucleus of ACs that failed to

invade (mean C/N: 0.157, n=41 animals) and only a single non-invasive AC was observed (**Fig 4 D, E**). In contrast, following treatment with *swsn-8*(*RNAi*) the majority of ACs that failed to invade the BM were in the G_1/S phases of the cell cycle based on CDK sensor ratiometric quantification (mean C/N: 0.636, n=21 animals) (**Fig 4 C, E**). Loss of expression of the core ATPase of the SWI/SNF complex through treatment with *swsn-4*(*RNAi*) resulted in variable localization of the CDK-sensor and a broad range of C/N ratios (C/N min: 0.240, C/N max: 1.140, n≥40 animals) in non-invasive single or mitotic ACs. Importantly, 14% (8/58) of ACs that failed to invade the BM following *swsn-4(RNAi)* treatment were present in the G_0 phase (C/N ratio < 0.3) of the cell cycle (**Fig 4 B, E**). This result reemphasizes the dependence of both SWI/SNF BAF and PBAF assemblies on the core ATPase of the complex, as the phenotype in the AC following *swsn-4(RNAi)* treatment appears to be a combination of the phenotypes seen in the *pbrm-1(RNAi)* and *swsn-8(RNAi)* conditions. While previous work in our lab, based on localization of a DNA licensing factor, CDT-1, has demonstrated indirectly that ACs must arrest in a G_0/G_1 cell cycle state (22,24), we lacked a sensitive enough tool to distinguish between these two interphase states. From our recent work utilizing a CDK sensor to examine the proliferation-quiescence decision in *C. elegans*, we can distinguish between pre-terminal cells in the somatic gonad in G_1 (mean C/N ratio: 0.67+/-0.10) as compared to terminally differentiated G_0 uterine cells (mean C/N ration: 0.30+/-0.11) (35). Here, our CDK activity measurements in the ACs of control animals provide the first quantitative demonstration that ACs arrest in a CDK^{low} G_0 state (**Fig S5 C**; mean control AC C/N ratio: 0.226+/-0.076) in order to invade. Furthermore, by combining the CDK sensor with loss of SWI/SNF subunits, our data indicate that the

SWI/SNF BAF assembly is specifically responsible for regulation of G_0 cell cycle arrest in the AC.

Forced G_0 arrest through ectopic CKI-1 rescues invasive potential in BAF-deficient but not PBAF-deficient ACs

We have previously proposed and characterized a dichotomy that exists between invasion and proliferation in the AC (22,24). As evidence of this, loss of two of the three TFs (*nhr-67*/Tlx and *hlh-2*/Daughterless) that function in a cell cycle-dependent manner to maintain the AC in a cell cycle-arrested state can be rescued through induced expression of a cyclin dependent kinase inhibitor, *cki-1* (p21/p27) (22). These results suggest that, at least in some cases, TF activity can be bypassed completely to promote AC invasion by maintaining G_0 arrest through direct cell cycle manipulation. To determine the extent to which the BAF complex contributes to AC invasion through regulation of cell cycle arrest, we used a heat-shock inducible transgene to ectopically express CKI-1::mTagBFP2 in SWI/SNF-deficient ACs (**Fig 5**). Since the heat shock inducible transgene is ubiquitous and expresses variably between different animals and different tissues within an individual animal, we limited our analysis to animals with ACs with obvious mTagBFP2 fluorescence expression. While forced arrest in G_0 was insufficient to significantly rescue AC invasion in animals treated with *swsn-4(RNAi)* (**Fig 5 B, B', E**) or *pbrm-1(RNAi)* (**Fig 5 D, D', E**), ectopic *cki-1* (CKI-1::mTagBFP2) expression in the AC strongly rescued cellular invasion in animals treated with *swsn-8(RNAi)* (**Fig 5 C, C', E**). Strikingly, in 85.7% (6/7) of animals treated with *swsn-8(RNAi),* forced G_0 arrest in ACs that had proliferated prior to ectopic CKI-1 expression

led to mitotic ACs breaching the BM (**Fig 5 F**), a phenotype we have reported previously using CKI-1 overexpression paired with loss of NHR-67. This demonstrated that mitotic ACs maintain the capacity to invade if they are re-arrested into a G_0 state (24). To corroborate our CKI-1 heat shock data, we used a lineage-restricted CKI-1 transgene (*cdh-3>CKI-1::GFP*) to induce G_0 cell cycle arrest in *swsn-4-* and *swsn-8-* depleted ACs (**Fig S6**). Similar to the heat shock results, lineage-restricted expression of CKI-1::GFP failed to rescue invasion in animals deficient in *swsn-4* (**Fig S6 A-B**). However, transgenic *cdh-3>CKI-1::GFP* animals treated with *swsn-8(RNAi),* had invasion defects significantly lower than control animals treated with *swsn-8(RNAi)* which lacked the G_0 rescue transgene (**Fig S6 B**). Altogether, these data corroborate our DHB-based CDK sensor data (**Fig 4**), suggesting that the SWI/SNF assemblies differentially contribute to AC invasion with BAF specifically required for G_0 cell cycle arrest.

SWI/SNF regulates chromatin state to promote pro-invasive gene expression in the AC GRN

Previous work has demonstrated that the gene regulatory network (GRN) that promotes AC invasion consists of both cell cycle-dependent and cell cycle-independent TF subcircuits (22,66) (**Fig 1 B**). In the cell cycle-dependent subcircuit of the TF-GRN, *egl-43* (EVI1/MEL), *hlh-2* (E/Daughterless), and *nhr-67* (TLX/Tailless) cooperate in a type 1 coherent feed-forward loop that is reinforced via positive feedback to retain the AC in a post-mitotic, invasive state (22,66). The cell cycle-independent subcircuit of the AC TF-GRN is governed by the *fos-1* (FOS) TF with feedback from both *egl-43* and *hlh-2* (22). Since loss of SWI/SNF expression in the AC results in both single and multiple

cells expressing the AC reporter, we treated endogenously GFP-labeled strains for each TF in the GRN with *swsn-4(RNAi)* to determine whether the SWI/SNF complex modulates the chromatin states of regulatory regions of these genes to contribute broadly to the regulation of either or both subcircuits (**Fig 6**). In the cell cycle-dependent subcircuit, knockdown of the SWI/SNF ATPase resulted in the most significant loss of expression of *egl-43::GFP* and *nhr-67::GFP* in the AC (39.19% and 25.97% GFP depletion, respectively; n≥40 animals; **Fig 6 A,C,E**). No significant difference was detected in the mean fluorescence expression of *GFP::hlh-2* in the AC upon knockdown of *swsn-4,* however the range of expression was much broader following *swsn-4(RNAi)* treatment (-2.32% GFP depletion; n=45 animals; **Fig 6 B,E**). In the cell cycle-independent subcircuit, loss of the SWI/SNF complex following treatment of *fos-1::GFP* animals with *swsn-4* RNAi resulted in a more moderate depletion of expression in the AC (10.6% GFP depletion; n=53 animals; **Fig 6 D**). These results suggest that the SWI/SNF complex likely contributes to AC invasion via remodeling chromatin states in enhancers and/or promoters of lineage-specific TFs in both cell cycle-dependent and -independent regulatory subcircuits that govern AC invasion.

The PBAF assembly regulates AC contact with underlying BM

Previous investigations into SWI/SNF have demonstrated divergent roles for the PBAF assembly in cell cycle regulation. In yeast, Remodeling the Structure of Chromatin (RSC), the homologous complex to PBAF, is required for progression through mitosis (68,69). In *Drosophila,* the homologous complex PBAP is not required and cell cycle progression and G_2/M transition is solely regulated by the BAF/BAP assembly (51). In

the *C. elegans* M lineage, RNAi-mediated loss of BAF results in hyperproliferation of the developing tissue, whereas knockdown of PBAF-specific subunits has little effect on cell cycle control (34). Similarly, in this study, RNAi-mediated loss of PBAF subunits *pbrm-1*, *swsn-7*, and *swsn-9* only resulted in single non-invasive cells expressing the AC reporter.

Given the discrepancy in knockdown efficiency between *pbrm-1(RNAi)* and RNAi targeting either the ATPase or BAF subunits in the AC (**Fig S4**) and the dose-dependent phenotype following loss of SWI/SNF ATPase (**Fig 3**), we next sought to determine whether strong loss of PBAF expression contributes to the extra AC phenotype. We used an auxin inducible degron (AID)-RNAi combination knockdown strategy to achieve strong PBAF depletion (70,71). We generated a strain with *pbrm-1* endogenously labeled with mNeonGreen and an AID (PBRM-1::mNG::AID) in a genetic background containing AC (*cdh-3>mCherry::moeABD*) and BM (*laminin::GFP*) reporters. We then quantified fluorescence expression in the AC in this strain. When grown under standard conditions, 6.45% of the ACs had not invaded the BM by the P6.p 4 cell stage, suggesting a partial loss of function of *pbrm-1* (n=31; **Fig 7 A, E-F**). This partial loss of function phenotype is likely due to the insertion of the mNG::AID tag into the genomic locus, putatively causing a hypomorphic allele, as has been reported for other knock-in alleles. Next, we introduced a ubiquitous, mRuby-labeled TIR1 transgene (*eft-3>TIR1::mRuby*) into the animals and assessed AC invasion under standard conditions and in the presence of the auxin hormone (auxin(+); **Fig 7 B**). We observed no statistically significant difference in the fluorescence expression of PBRM-1::mNG::AID protein in the AC, nor did we observe any differences in AC invasion

between the strains with and without the TIR1 transgene when grown on media in the absence of auxin (auxin(-)) (TIR1+: 3.17% depletion, 16.67% invasion defect; n=30; **Fig 7 E-F**). However, in both conditions, some ACs that invaded seemed to do so only partially, as most of the ventral epidermal BM remained intact beneath ACs (**Fig 7 B**, black arrow). In the auxin(+) condition, there was a significant reduction in PBRM-1::mNG::AID protein level in the AC of animals containing the TIR1 transgene relative to the same strain grown in the auxin(-) condition or the strain without the TIR1 transgene (49.26% and 50.87%, respectively; n=30; **Fig 7 E**), though there was no significant difference in the penetrance of AC invasion defects (16.67% invasion defect; n=30; **Fig 7 F**). Similar to our previous results with *pbrm-1(RNAi)* treated animals, no extra ACs were noted following loss of expression of PBAF in the AC using the AID system.

Since the PBAF assembly in *C. elegans* consists of several subunits, *pbrm-1* (PBRM1), *swsn-7* (ARID2), and *swsn-9* (BRD7/BRD9), we next investigated whether combinatorial knockdown of PBAF subunits would enhance the penetrance of AC invasion defects and lead to extra ACs. To accomplish this, we treated *pbrm-1::mNG::AID* animals containing ubiquitous TIR1 with our improved *swsn-7(RNAi)* or *swsn-9(RNAi)* in both auxin(+) and auxin(-) conditions. In the auxin(-) condition, there was no significant difference in PBRM-1::mNG::AID expression in the AC of animals treated with *swsn-7(RNAi)* compared to animals treated with empty vector control (n=30; **Fig 7 E**), however there was markedly less AC invasion (50.00% invasion defect; n=30; **Fig 7 F**). Strikingly, in one case, the AC was completely detached from the BM, as we detected no AC membrane protrusions (*cdh-3>mCherry::moeABD*) in contact with the ventral surface of the gonad (**Fig 7 F**). Animals treated with *swsn-7(RNAi)* and

auxin(+) had significantly lower expression of PBRM-1::mNG::AID in the AC when compared to animals treated with *swsn-7(RNAi)* in the auxin(-) condition (48.50% depletion; n=30; **Fig 7 E**). While no significant difference was seen in loss of AC invasion in auxin(+) (48.39% AC invasion defect), 16% (5/31) of animals in this treatment had ACs entirely detached from the ventral BM (n=31; **Fig 7 F-G**). In contrast to treatment with *swsn-7(RNAi)*, in the *swsn-9(RNAi)* auxin(-) condition, PBRM-1::mNG::AID expression in ACs was significantly lower than that in the ACs of animals treated with empty vector control auxin(-) (38.69% depletion; n=30; **Fig 7 E**). However, there was still a significant decrease in expression of *pbrm-1::mNG::AID* in ACs in *swsn-9(RNAi)* auxin(+) compared to the *swsn-9(RNAi)* auxin(-) condition (19.14% depletion; n=30; **Fig 7 E**), though we saw no statistically significant difference in penetrance of AC invasion defects between the two conditions (30.00% vs. 43.33%; n=30; **Fig 7 F**). We also noted one animal with a detached AC in the *swsn-9(RNAi)* auxin(-) condition and zero in the auxin(+) condition (**Fig 7 F**). Additionally, we only observed one AC per animal across all of these treatments, supporting the hypothesis that PBAF does not contribute to cell cycle arrest in the AC.

Detached ACs in both the *swsn-7(RNAi)* and *swsn-9(RNAi)* AID combination knockdown conditions suggest that the PBAF assembly regulates AC contact with the ventral epidermal BM. A previous study has shown that AC attachment is regulated by the *fos-1/egl-43* cell cycle-independent subcircuit of the AC GRN via regulation of lamellipodin/*mig-10b* and non-autonomously via netrin/*unc-6* signaling (72). ACs deficient in components of this pathway are attached to the ventral epidermal BM when specified and gradually lose contact over time, with peak loss of contact occurring at the

time of AC invasion at the P6.p 4-cell stage (72). In order to determine whether PBAF remodels chromatin to promote activation of this subcircuit of the AC GRN, we treated endogenously tagged *fos-1::GFP* (22) animals with *pbrm-1(RNAi)* and quantified fluorescence expression in ACs that displayed invasion defects (**Fig S7 A-B**). ACs deficient in *pbrm-1(RNAi)* had a modest but statistically significant loss of FOS-1::GFP protein levels in non-invasive ACs (33.60% depletion; n=20; **Fig S7 B**), suggesting that the PBAF assembly partially regulates the *fos*-dependent pathway that mediates attachment to the underlying BM.

As PBAF complex depletion resulted in moderate loss of FOS-1::GFP in the AC, we next examined functional interactions between FOS-1 and PBRM-1. Given that the PBRM-1::mNG::AID allele was slightly hypomorphic, with ~6% and ~17% invasion defects in backgrounds without or with TIR1, respectively, we used this strain as a sensitized background. We found that even without the addition of auxin, co-depletion with *fos-1(RNAi)* resulted in almost complete loss of AC invasion (96.77% invasion defect; n=31; **Fig S7 C-D**). Finally, we examined whether RNAi-mediated depletion of *pbrm-1* is synergistic with loss of downstream targets of FOS-1, the matrix metalloproteinases (MMPs). Previously, it has been shown that animals harboring null mutations for five of the six MMPs encoded in the *C. elegans* genome (*zmp-1,-3,-4,-5* and *-6*), show delayed AC invasion (21). RNAi depletion of *pbrm-1* in quintuple MMP mutants significantly and synergistically enhanced late invasion defects (scored at the P6.p 8-cell stage) in this background (24.24% invasion defect; n=33; **Fig S7 E-F**) as compared to loss of either PBAF (3.8%; n=50) or MMPs (0%; n=30) alone. Together,

these results suggest that the PBAF complex functions through modulation of chromatin state, synergistically with FOS-1 to regulate AC invasion.

DISCUSSION

A tissue-specific CRF RNAi screen identified genes critical for cellular invasion

A complex dialog between microenvironmental cues, activation of pro-invasive GRNs, and subsequent remodeling of the BM dictates a cell's ability to adopt an invasive phenotype (22,73). Broad regulation of cell behavioral programs like invasion through BMs requires modulation of chromatin states in the regulatory regions of hundreds of genes. Previous work in the *C. elegans* AC and in cancer cell invasion has emphasized the necessity for chromatin regulating factors in the promotion of cellular invasion (24,74–78). In this study, we used the *Caenorhabditis elegans* AC invasion model as a single cell, *in vivo* system to identify a suite of CRFs that contribute to the process of cellular invasion. We performed a tissue-specific RNAi feeding screen to assess 270 genes implicated in chromatin binding, chromatin remodeling complexes, or histone modification. We do not claim that genes that we failed to identify as strong regulators of cellular invasion in the screen are unimportant for the process; however, RNAi-mediated loss of the majority of CRF genes did result in some penetrance of AC invasion defects (**Table S1**). This finding was expected, as many of the genes we screened are global regulators of the genome and broadly contribute to various cell biological processes. We extracted a list of the most penetrant regulators of cell invasion from the broader list (**Table S2**). Many genes and gene classes that we recovered as significant regulators of AC invasion are homologous to human genes that

have been previously studied in the context of cellular invasion and tumorigenesis including *cec-6*/CBX1/CBX8 (77,79), *cfi-1*/ARID3A/ARID3C (80), *psr-1*/JMJD6 (81), *lin-35*/RB1/RBL (82,83), *skp-1*/SNW1 (84), and several TAFs (*taf*-1/TAF1/TAF1L, taf-*5*/TAF5/TAF5L, *taf-7.1*/TAF7/TAF7L) (83,85,86). Additionally, we recovered nematode-specific genes *nra-3, and cec-2,* and two genes, *cec-3* (homologous human protein is uncharacterized) and *gna-2*/GNPNAT, whose human homologs have not been previously studied in the context of cellular invasion to our knowledge. As the majority of the CRF genes we identified as significant regulators of AC invasion have been previously studied in the context of invasion in human development and cancer metastasis, these results demonstrate the credibility of the *C. elegans* AC invasion system as a genetically and optically tractable *in vivo* environment to corroborate and characterize previously identified CRFs that promote cellular invasion in human diseases such as rheumatoid arthritis and cancer. Future studies should continue to characterize the relationship between CRFs identified here and cellular invasion.

The dose of SWI/SNF ATPase dictates the severity of AC invasion and G_0 arrest defects

For the majority of this study, we focused on characterizing the contribution of the SWI/SNF ATP-dependent chromatin remodeling complex to cellular invasion because it was highly represented among our list of significant regulators of AC invasion and has been extensively studied in the context of both cellular invasion and cell cycle control across a variety of animal models and in human cancers (30,34,39,41,47,53,57,78,87–92). The SWI/SNF complex is a highly conserved eukaryotic chromatin remodeler that

is generally associated with activating chromatin states and antagonism of the Polycomb repressive complex (PRC) (25,93). Prior whole-exome studies have determined that over 20% of human tumors harbor mutations in one or more subunits of the SWI/SNF complex (31,47,94). Despite the high frequency of SWI/SNF mutations, the distribution of mutations is non-random across the array of cancers, and mutation of specific subunits has been strongly linked to individual cancer subtypes (31,94). One of the most frequently mutated subunits of the complex across SWI/SNF-deficient cancers is the core ATPase subunit BRG1/SMARCA4 (47,95). Aberrant expression of BRG1 has been studied in the context of a variety of malignancies, including lung (96,97) and ovarian small cell carcinomas (98). BRM/SMARCA2, the mutually exclusive ATPase paralog to BRG (76), is also a frequent target for mutation and aberrant expression in tumorigenesis (31,94,99).

Due to the high degree of similarity in structure between BRG and BRM, mutation or epigenetic silencing of either ATPase can be compensated by expression of the other. Previous investigation has determined BRM to be an effective synthetic lethal target in BRG1-deficient cancer, and vice-versa (100,101). The wide spectrum of phenotypic severity seen in both intellectual disorders and cancers that result from mutated or altered expression of the SWI/SNF ATPases is dependent on the dose of functional SWI/SNF in affected tissues (31,33). Levels of BRG1 have been used as specific, context-dependent prognostic indicators, especially in cancer. In breast cancer, low expression of BRG1 is associated with better patient outcomes (30), whereas increased expression of BRG1 has been linked to increased tumor growth and cellular invasiveness in the context of hepatocellular carcinoma (32). Despite the compensatory

nature of BRG1/BRM in many tumorigenic contexts, concomitant loss of expression of both ATPases has been described in metastatic murine models and patient-derived non-small-cell lung cancer (NSCLC) cell lines and is associated with poor patient survival (87,102,103).

In *C elegans*, the sole SWI/SNF ATPase, *swsn-4,* has a high degree of homology to both mammalian BRG1 and BRM, providing a unique opportunity to accessibly model the connection between dual loss of BRG1/BRM associated with poor prognostic outcomes in NSCLC and cellular invasion in the AC. A recent study demonstrated a phenotypic dosage-sensitivity following loss of SWI/SNF expression in relation to terminal differentiation of *C. elegans* muscle and vulval tissues (34). In early M cell development, the mesodermal lineage that gives rise to BWM, SM, and coelomocytes (104), RNAi knockdown targeting subunits *swsn-1* (SMARCC1/2) or *swsn-4* (BRG1/BRM) did not affect cell cycle exit. However, strong loss of expression of either core subunit using a lineage-specific knockout strategy in the M cell descendants resulted in extra BWM cell divisions (34). In contrast to these results from early M cell development, later in larval development, RNAi-mediated knockdown of the SWI/SNF core resulted in hyperproliferation of M lineage descendants, whereas gene knockouts resulted in hypoproliferation of the tissue (34). These results demonstrate that the context- and dose-dependent relationship seen in mammalian development and SWI/SNF-deficient cancers may represent a more general behavior of the complex.

Our data here using a combination of an improved *swsn-4* RNAi vector with an anti-GFP-targeting nanobody construct demonstrates that cellular invasion and cell cycle control depend on the dose of functional SWI/SNF ATPase present in the AC at

the time of invasion. In addition to reflecting the dose-dependent nature of the SWI/SNF ATPase in cancer, our data in the AC is consistent with work done in *C. elegans* early mesoblast development where complete loss of the *swsn-4* ATPase using a catalytically dead mutant and lineage-specific knockout strategy results in loss of cell cycle arrest (34). A limitation to our experimental strategy is that we cannot be sure that combining *swsn-4* RNAi with an anti-GFP-targeting nanobody to deplete the SWI/SNF ATPase represents a null phenotype, as we limited our analysis to quantitative fluorescence measurements. However, we show that treatment with the improved *swsn-4(RNAi)* vector alone is sufficient to phenocopy the null phenotype previously reported in late mesoblast (sex myoblast, SM) development (**Fig S5**). Additionally, enhancement of the AC mitotic phenotype statistically tracked with a progressive step down in mean expression of the ATPase in the AC across our experiments. Using endogenous fluorescent reporters, we also provide evidence that the SWI/SNF complex broadly regulates both cell cycle- dependent and -independent subcircuits of the AC GRN (**Fig 6**). Altogether, this data supports the hypothesis that SWI/SNF contributes to cell cycle control in a dose-dependent manner and provides the first line of evidence to link SWI/SNF ATPase dosage to the dichotomy between invasion and proliferation (**Fig 7 H**).

The SWI/SNF BAF complex promotes cellular invasion through induction of G_0 cell cycle arrest

The SWI/SNF complex is composed of an ATPase-containing core and accessory factors, which collectively, provide a platform of common factors bound by

assembly-specific subunits in a mutually exclusive manner. In *C. elegans*, the binding of SWSN-8 (BAF250a/ BAF250b/ ARID1A/ ARID1B) and DPFF-1 (BAF45b/ BAF45c/ BAF45d/ DPF3) to the common factors forms the SWI/SNF BAF complex. Since we identified representative subunits from the core of the complex and both SWI/SNF BAF and PBAF assemblies in our CRF RNAi screen, we took a cell biological and genetic approach to investigate the role of the each SWI/SNF assembly in promoting cellular invasion. Here, using a DHB-based CDK sensor (35,67), we show that loss of either the core of the complex or the BAF complex specifically results in mitotic ACs that failed to invade the BM. Our cell cycle sensor data suggests first that the wild-type AC invades in a G_0 CDK^{low} state, and second, that the main contribution of the BAF assembly to AC invasion is through maintenance of this G_0 arrest, as many ACs that failed to invade the BM had increasing CDK activity, indicative of cells cycling in S or G_2. Alternatively, 14% of ACs that failed to invade the BM following loss of *swsn-4*/ATPase of the complex had CDK activity ratios indicative of G_0 cell cycle arrest, suggesting a cell cycle-independent defect. In support of this, forced arrest of BAF-deficient ACs in G_0 was sufficient to significantly rescue invasion, whereas CKI-1 induction failed to rescue invasion in ACs deficient in *swsn-4*/ATPase. Altogether, our results indicate that the major contribution of the SWI/SNF complex to AC invasion is through regulation of G_0 cell cycle arrest via the BAF assembly. Future investigation will require biochemical techniques to determine a mechanistic explanation for how exactly the BAF complex regulates the chromatin landscape of cell cycle regulators to promote invasion. Targeted DNA adenine methyltransferase identification (TaDa) is an attractive biochemical approach that may be adaptable to the AC invasion system. This approach has been characterized as an

effective, tissue-specific method to identify TF-target sequence interactions in the *C. elegans* epidermis (105).

The PBAF complex regulates AC invasion and attachment to the BM

The *C. elegans* PBAF assembly consists of the PBRM-1/BAF180, SWSN-7 (BAF200/ARID2), and SWSN-9 (BRD7/BRD9) subunits bound to the SWI/SNF common factors (core and accessory subunits). Previous work in *C. elegans* has not revealed a connection between the PBAF assembly and cell cycle arrest. Our initial experiments with improved PBAF RNAi vectors resulted in a weaker penetrance of AC invasion relative to loss of the core or BAF assembly and our cell cycle sensor data suggested that ACs deficient in PBAF, that fail to invade the BM, remain in a G_0 cell cycle state. Thus, our data shows no PBAF contribution to cell cycle control in the AC. We used the auxin inducible degron (AID) system to robustly deplete PBRM-1 in the PBAF assembly and combined loss of *pbrm-1* with enhanced RNAi-mediated knockdown of the other two PBAF subunits, *swsn-7* and *swsn-9*. This combination knockdown strategy corroborated our previous results as we saw no significant penetrance of extra ACs. Rather, here we associate a striking AC detachment phenotype with strong knockdown of the PBAF assembly. We also note aberrant BM morphology in some ACs deficient in PBAF, with only one of the two BMs removed, suggesting that this assembly regulates attachment and extracellular matrix (ECM) remodeling in wild-type ACs to promote invasion, potentially through the regulation of HIM-4/Hemicentin, an extracellular immunoglobulin-like matrix protein that functions in the AC to fuse the two BMs through the formation of novel BM-BM adhesion, the B-LINK (106). Finally, although PBAF

depletion partially depleted levels of FOS-1::GFP, a key TF responsible for the expression of MMPs and other pro-invasive targets, we detected significant enhancement of invasion defects from depleting FOS-1 in a hypomorphic *pbrm-1* background and reciprocally, depletion of PBRM-1 enhanced the invasion defect of the quintuple MMP mutant. As we did see multiple cases of AC-BM detachment following PBAF depletion, we suspect that PBAF functions synergistically with FOS-1 to facilitate chromatin remodeling of pro-invasive genes required for BM attachment. Collectively, these results reveal a distinct contribution for each SWI/SNF assembly to the process of cellular invasion and reiterate the dependence of each assembly on the functional dose of ATPase in a cell.

ACKNOWLEDGEMENTS

We are thankful to David Gray, Ed Luk, Laura Mathies, Benjamin Martin, Robert Morabito, Valerie Reinke, Courtney Tello, and Gerald Thomsen for advice and comments on this manuscript. Some *C. elegans* strains were provided by the CGC, which is funded by NIH Office of Research Infrastructure Programs (P40 OD010440).

AUTHOR CONTRIBUTIONS

J.J.S. and D.Q.M. designed the experiments. J.J.S., Y.X., and M.A.Q.M. performed the experiments. J.J.S., A.Q.K., F.E.Q.M., M.C., N.P., and Y.X. organized and performed the RNAi screen. J.J.S., A.Q.K., S.L., T.N.M.-K., Y.X., K.W. and P.K generated strains. J.J.S performed the data analysis and prepared the manuscript with feedback from other authors. J.J.S. and D.Q.M acquired funding for the completion of this project.

DECLARATION OF INTERESTS

The authors declare no competing interests.

FUNDING

This work was funded by the National Institute of General Medical Sciences (NIGMS) [1R01GM121597-01 to D.Q.M.]. D.Q.M. is also a Damon Runyon-Rachleff Innovator supported (in part) by the Damon Runyon Cancer Research Foundation [DRR-47-17]. J.J.S was supported by an NIH/NIGMS Diversity Supplement [3R01GM121597-02S1] and the W. Burghardt Turner Fellowship. M.A.Q.M. [3R01GM121597-03S1] and F.E.Q.M. [3R01GM121597-04S1] are supported by an NIH/NIGMS Diversity Supplement. T.N.M.-K. is supported by the NIH/NICDH [F31HD100091-01].

FIGURE LEGENDS

Figure 1. Summary of *C. elegans* AC invasion through the underlying BM and AC GRN.

(A) Schematic depicting AC invasion in the mid-L3 stage of *C. elegans* development (left) and micrographs demonstrating the coordination of AC (magenta, *cdh-3>PH::mCherry*) invasion through the BM (green, *laminin::GFP*) with primary vulval development. The fluorescent AC-specific membrane marker and BM marker are overlaid on DIC in each image. In this and all other figures, white arrowheads indicate AC(s), yellow arrowheads indicate boundaries of breach in BM, and white brackets

indicate 1° VPCs. Scale bar, 5 µm. **(B)** Overview of the transcription factor network governing AC invasion, which consists of cell cycle-independent (*fos-1*) and dependent (*egl-43, hlh-2,* and *nhr-67*) subcircuits, which together with *hda-1* promote pro-invasive gene expression and maintain AC cell cycle arrest.

Figure 2. Enhanced RNAi targeting SWI/SNF core, BAF, and PBAF complexes results in penetrant invasion defects.

(A) Schematic depicting the *C. elegans* SWI/SNF core (middle, green), accessory (middle, gray), BAF (left, blue), and PBAF (right, orange) assemblies. **(B-D)** DIC (left), corresponding fluorescence images (middle), and fluorescence overlay (right) representing loss of AC (magenta, *cdh-3>mCherry::moeABD*) invasion through the BM (green, *laminin::GFP*) following RNAi depletion of SWI/SNF core (*swsn-1* and *swsn-4*) **(B)**, BAF (*swsn-8*) **(C)**, and PBAF (*pbrm-1, swsn-7,* and *swsn-9*) **(D)** subunits. In cases where multiple cells expressed the AC reporter (2+ACs) in the same animal, each is indicated with a white arrowhead. A representative image of a single AC that fails to breach the BM is displayed as an inset (white dashed box, bottom left). **(E)** Stacked bar chart showing the penetrance of AC invasion defects following treatment with SWI/SNF RNAi depletion, binned by AC phenotype (n≥50 animals examined for each treatment). Scale bar, 5 µm.

Figure 3. AC invasion and G_0/G_1 cell cycle arrest depend on dosage of SWI/SNF ATPase.

(A-E) Representative fluorescence images depicting expression of BM marker (*laminin::GFP*) and endogenous SWSN-4::GFP (left), AC reporter (*cdh-3>mCherry::moeABD*) and anti-GFP nanobody (*anti-GFP-nano-mCherry::HIS*) (middle),

and fluorescence overlay (right) across experimental treatments. In cases where multiple cells expressed the AC reporter in the same animal, each is indicated with a single white arrowhead. Asterisk indicates anti-GFP nanobody expression in neighboring VU cells. Scale bar, 5 µm. **(F)** Quantification of mean gray values (M.G.V.) of endogenous SWSN-4::GFP in ACs in control animals (empty vector) and across all experimental treatments normalized to mean fluorescent expression in wildtype animals (n≥40 animals per treatment, p values for Student's *t*-test comparing expression of successive knockdown are displayed on the figure). In this and all other figures, open circles and error bars denote mean±standard deviation (s.d.). **(G)** Stacked bar chart showing quantification of AC invasion defects corresponding to each treatment, binned by AC phenotype (n≥40 animals per condition; p values for Fisher's exact test comparing phenotypes of successive knockdown strategies are displayed above compared groups). Grey brackets indicate statistical significance between invasion total in each condition compared to invasion defect total. Black brackets indicate statistical significance between incidences of invasion defects with multiple ACs compared to incidences of invasion defects with single ACs.

Figure 4. CDK sensor reveals SWI/SNF contribution to G_0 arrest in the AC. Micrographs depicting DIC (left), AC (*cdh-3>mCherry::moeABD*, center-left), DIC overlay (center-right), and DHB-based CDK activity sensor (right) in empty vector **(A)** and following treatment with SWI/SNF RNAi targeting the core **(***swsn-4***, B)**, BAF **(***swsn-8***, C)** and PBAF **(***pbrm-1*, **D)** assemblies of the complex. In cases where treatment resulted in multiple cells expressing the AC reporter in the same animal, representative images of both single (1AC) and mitotic (2+ACs) phenotypes are given, and each AC is

indicated with a single white arrowhead. Quantification of the cytoplasmic:nuclear (C/N) ratio of DHB::GFP in ACs (white dotted outline) is listed in the bottom left of each panel. Mitotic ACs are numbered, and C/N ratios are provided for each **(B-C)**. White arrow in C indicates an AC that is out of the focal plane. Scale bar, 5 µm. **(E)** Quantification of C/N DHB::GFP ratios for all ACs in empty vector control and each RNAi treatment (n≥30 animals per treatment). Mean C/N ratio is represented by colored open circles and correspond to numbers of the same color. Gradient scale depicts cell cycle state as determined by quantification of each AC in all treatments (n≥30 animals per treatment), with dark-black depicting G_0 and lighter-magenta depicting G_2 cell cycle states. Dashed white line on gradient scale bar (right) corresponds to boundaries between G_0 and G_1 phases.

Figure 5. BAF depletion is rescued by G_0/G_1 arrest.

Representative micrographs depicting DIC (left), BM (*laminin::GFP*, center-left), AC (*cdh-3>mCherry::moeABD,* center-right), and CKI-1 (*hsp>CKI-1::mTagBFP2*) expression in empty vector control **(A-A')** and treatment with SWI/SNF RNAi under standard conditions **(A-D)** and following heat shock induction of CKI-1 **(A'-D')**. CKI-1 images have been inverted for ease of visualization. **(E)** Stacked bar chart showing percentage of AC invasion defects corresponding to each RNAi treatment under standard growth conditions (control) and following heat shock induction of CKI-1 (+CKI-1), binned by AC phenotype (n≥30 animals per condition; Fisher's exact test compared CKI-1(+) animals with control, non-heat shocked animals; p value is displayed above compared groups). **(F)** Representative micrographs of invasive group of *swsn-8* deficient ACs following induction of G_0/G_1 arrest. DIC (top-left), BM (bottom-left), CKI-1

expression (top-right), AC reporter (bottom-right). Max intensity z-projection of AC and BM reporter channels (bottom). Large breach in BM is indicated by black arrow. Scale bar, 5 µm.

Figure 6. SWI/SNF regulates endogenously tagged TFs in the AC invasion GRN. Fluorescent micrographs depicting expression of endogenously tagged TFs in the cell cycle-dependent subcircuit (*egl-43::GFP* **(A),** *GFP::hlh-2* **(B),** and *nhr-67::GFP* **(C)**) and cell cycle-independent subcircuit (*GFP::fos-1a* **(D)**) of the AC GRN in animals treated with empty vector control (left) or *swsn-4(RNAi)* (right). Scale bar, 5 µm. **(E)** Quantification of fluorescent expression of each TF::GFP in ACs of control animals and animals treated with *swsn-4(RNAi)*. Statistical comparisons were made between the expression of each TF subunit in the AC in control and RNAi-treated animals using Student's *t*-test (n≥30 for each condition; p values are displayed above black brackets).

Figure 7. PBAF promotes AC contact to the BM.

Representative micrographs of BM (*lam::GFP*) and endogenous *pbrm-1::mNG::AID* (left), AC (cdh-3>mCherry::moeABD, center), and fluorescent overlays (right) of animals lacking **(A)** or possessing **(B-D)** ubiquitous TIR1 expression treated with empty vector control **(B)** or RNAi targeting PBAF subunits in the absence Aux(-) (top) or presence Aux(+) (bottom) of media containing the auxin hormone **(C-D). (E)** Quantification of fluorescence expression (M.G.V) of PBRM-1::mNG::AID in ACs of animals in each condition (N≥30 animals in each treatment; p values for Fisher's exact test comparing strains containing TIR1 to the TIR1(-) strain, and comparing strains containing TIR1 in the Aux(-) to the Aux(+) condition, are displayed above compared groups). **(F)** Stacked bar chart showing percentage of AC invasion defects corresponding to each treatment,

binned by AC phenotype (N≥30 animals per condition). Black brackets indicate statistical significance between invasion total in each condition compared to invasion defect total. **(G)** Max intensity z-projection of AC and BM reporter channels depicting a detached AC phenotype in *swsn-7*-deficient ACs in the Aux(+) condition. BM (left), AC (center), fluorescence overlay (right). Asterisk indicates polarized F-actin driven protrusion extending ventrally. **(H)** Schematic summary of the how the SWI/SNF PBAF (orange – *swsn-7* (7), *swsn-9* (9), *pbrm-1* (P)) and BAF (*swsn-8* (8), *dpff-1* (D)) assemblies contribute to AC invasion.

MATERIALS & METHODS

C. elegans strains and culture conditions

All animals were maintained under standard conditions and cultured at 25°C, except strains containing temperature-sensitive alleles *swsn-1(os22), swsn-4(os13)*, and the uterine-specific RNAi hypersensitive strain used in the chromatin remodeler screen containing the *rrf-3(pk1426)* allele, which were maintained at either 15°C or 20°C (107). The heat shock inducible *cki-1::mTagBFP2* transgene was expressed via incubating animals at 32°C for 2-3 hours in a water bath starting at the P6.p 2-cell VPC stage. Animals were synchronized for experiments through alkaline hypochlorite treatment of gravid adults to isolate eggs (108). In the text and figures, we designate linkage to a promoter through the use of the (>) symbol and fusion of a proteins via a (::) annotation.

Molecular biology and microinjection

SWI/SNF subunits *swsn-4* and *swsn-8* were tagged at their endogenous loci using CRISPR/Cas9 genome editing via microinjection into the early adult hermaphrodite syncytial gonad (109,110). Repair templates were generated as synthetic DNAs from

either Integrated DNA Technologies (IDT) as gene blocks (gBlocks) or Twist Biosciences as DNA fragments and cloned into *ccdB* compatible sites in pDD282 by New England Biolabs Gibson assembly (111). Homology arms ranged from 690-1200 bp (see **Tables S5** for additional details). sgRNAs were constructed by EcoRV and NheI digestion of the plasmid pDD122. A 230 bp amplicon was generated replacing the sgRNA targeting sequence from pDD122 with a new sgRNA and NEB Gibson assembly was used to generate new sgRNA plasmids (see **Table S5** for additional details). Hermaphrodite adults were co-injected with guide plasmid (50 ng/µL), repair plasmid (50 ng/µL), and an extrachromosomal array marker (pCFJ90, 2.5 ng/µL), and incubated at 25 ºC for several days before screening and floxing protocols associated with the SEC system (111).

RNA interference (RNAi)

All 270 RNAi clones assessed in the chromatin remodeler screen were derived from the commercially available Vidal RNAi library. Presence of inserts into the L4440 RNAi vector was confirmed via colony PCR amplification of all L4440 vectors used in the chromatin remodeler screen. Vectors which resulted in penetrant loss of invasion (see **Table S2**) were also sequenced to confirm the identity of the insert targeting chromatin remodeler genes in the L4440 vector using Sanger sequencing at the Genomics Core Facility at Stony Brook University. An RNAi sub-library of SWI/SNF subunits was constructed by cloning 950-1000 bp of synthetic DNA based on cDNA sequences available on WormBase (www.wormbase.org) into the highly efficient T444T RNAi vector (112,113). Synthetic DNAs were generated by Twist Biosciences as DNA fragments and cloned into restriction digested T444T using NEB Gibson Assembly (see

Tables S6 for additional details). For all experiments, synchronized L1 stage animals were directly exposed to RNAi through feeding with bacteria expressing dsRNA (114).

Auxin-mediated degradation

To combine RNAi with the depletion of AID-tagged proteins, 1 mM K-NAA was used, and its effects were analyzed as previously described(115). Briefly, L1 animals were first synchronized by sodium hypochlorite treatment and transferred to NGM plates seeded with the RNAi vector of interest. At the P6.p 1-cell stage, a time in development where the AC has already undergone specification, animals were transferred to RNAi-seeded plates treated with K-NAA. Animals were staged by DIC.

Live cell microscopy

All micrographs included in this manuscript were collected on a Hamamatsu Orca EM-CCD camera mounted on an upright Zeiss AxioImager A2 with a Borealis-modified CSU10 Yokagawa spinning disk scan head using 405nm, 488 nm, and 561 nm Vortran lasers in a VersaLase merge and a Plan-Apochromat 100x/1.4 (NA) Oil DIC objective. MetaMorph software (Molecular Devices) was used for microscopy automation. Several experiments and all RNAi screening were scored using epifluorescence visualized on a Zeiss Axiocam MRM camera, also mounted on an upright Zeiss AxioImager A2 and a Plan-Apochromat 100x/1.4 (NA) Oil DIC objective. Animals were mounted into a drop of M9 on a 5% Noble agar pad containing approximately 10 mM sodium azide anesthetic and topped with a coverslip.

Assessment of AC invasion

Both for the purposes of the CRF RNAi screen and all other experiments AC invasion was scored at the P6.p 4-cell stage, when 100% of wild-type animals exhibit a breach in

the BM (14). In strains with the laminin::GFP transgene, an intact green fluorescent barrier under the AC was used to assess invasion. Wild-type invasion is defined as a breach as wide as the basolateral surface of the AC (14). Raw scoring data is available in **Tables S1 and S4.**

Image quantification and statistical analyses

Images were processed using Fiji/ImageJ (v.2.1.0/1.53c) (116). Expression levels of SWSN-4::GFP, SWSN-8::GFP, PBRM-1::eGFP, and PBRM-1::mNG::AID were measured by quantifying the mean gray value of AC nuclei, defined as somatic gonad cells near the primary vulva expressing the *cdh-3>mCherry::moeABD* transgene. Background subtraction was performed by rolling ball background subtraction (size=50). For characterization of experiments involving SWI/SNF endogenous tags and AC GRN TFs::GFP treated with *SWI/SNF(RNAi)* and GFP-targeting nanobody the L3 stage, only animals exhibiting defects in invasion were included in the analysis. Data was normalized to negative control (empty vector) values for the plots in **Fig 3** and **Fig S8**. Quantification of either CDK cell cycle sensor (either DHB::GFP or DHB::2xmKate2) was performed by hand, as previously described (35). Images were overlaid and figures were assembled using Adobe Photoshop 2020 (v. 21.1.2) and Adobe Illustrator 2020 (v. 24.1.2), respectively. Statistical analyses and plotting of data were conducted using RStudio (v. 1.2.1335). Statistical significance was determined using either a two-tailed Student's t-test or Fisher's exact probability test. Figure legends specify when each test was used and the p-value cut-off.

REFERENCES

1. Rowe RG, Weiss SJ. Breaching the basement membrane: who, when and how? Trends Cell Biol. 2008;18(11):560–74.
2. Nourshargh S, Alon R. Leukocyte Migration into Inflamed Tissues. Immunity [Internet]. 2014;41(5):694–707. Available from: http://dx.doi.org/10.1016/j.immuni.2014.10.008
3. Medwig TN, Matus DQ. Breaking down barriers: the evolution of cell invasion. Curr Opin Genet Dev [Internet]. 2017;47:33–40. Available from: http://dx.doi.org/10.1016/j.gde.2017.08.003
4. Liu Y, Pan YF, Xue YQ, Fang LK, Guo XH, Guo X, et al. UPAR promotes tumor-like biologic behaviors of fibroblast-like synoviocytes through PI3K/Akt signaling pathway in patients with rheumatoid arthritis. Cell Mol Immunol [Internet]. 2018;15(2):171–81. Available from: http://dx.doi.org/10.1038/cmi.2016.60
5. Ye Y, Gao X, Yang N. LncRNA ZFAS1 promotes cell migration and invasion of fibroblast-like synoviocytes by suppression of miR-27a in rheumatoid arthritis. Hum Cell. 2018;31(1):14–21.
6. Hanahan D, Weinberg RA. Hallmarks of cancer: The next generation. Cell [Internet]. 2011;144(5):646–74. Available from: http://dx.doi.org/10.1016/j.cell.2011.02.013
7. Justus CR, Leffler N, Ruiz-Echevarria M, Yang L V. In vitro cell migration and invasion assays. J Vis Exp. 2014;(88):1–8.
8. Li BB, Scott EY, Dean Chamberlain M, Duong BTV, Zhang S, Done SJ, et al. Cell invasion in digital microfluidic microgel systems. Sci Adv. 2020;6(29).

9. Eibl G, Reber HA. A xenograft nude mouse model for perineural invasion and recurrence in pancreatic cancer. Pancreas. 2005;31(3):258–62.

10. Busuttil RA, Liu DS, Di Costanzo N, Schröder J, Mitchell C, Boussioutas A. An orthotopic mouse model of gastric cancer invasion and metastasis. Sci Rep. 2018;8(1):2–9.

11. Cheng B, Wang Q, Song Y, Liu Y, Liu Y, Yang S, et al. MIF inhibitor, ISO-1, attenuates human pancreatic cancer cell proliferation, migration and invasion in vitro, and suppresses xenograft tumour growth in vivo. Sci Rep. 2020;10(1):1–10.

12. Wen J, Yin P, Li L, Kang G, Ning G, Cao Y, et al. Knockdown of Matrix Metallopeptidase 9 Inhibits Metastasis of Oral Squamous Cell Carcinoma Cells in a Zebrafish Xenograft Model. Biomed Res Int. 2020;2020.

13. Guo Y, Fan Y, Pei X. Fangjihuangqi Decoction inhibits MDA-MB-231 cell invasion in vitro and decreases tumor growth and metastasis in triple-negative breast cancer xenografts tumor zebrafish model. Cancer Med. 2020;9(7):2564–78.

14. Sherwood DR, Sternberg PW. Anchor cell invasion into the vulval epithelium in C. elegans. Dev Cell. 2003;5(1):21–31.

15. Kelley LC, Lohmer LL, Hagedorn EJ, Sherwood DR. Traversing the basement membrane in vivo: A diversity of strategies. J Cell Biol. 2014;204(3):291–302.

16. Sherwood DR, Butler JA, Kramer JM, Sternberg PW. FOS-1 promotes basement-membrane removal during anchor-cell invasion in C. elegans. Cell. 2005;121(6):951–62.

17. Hagedorn EJ, Yashiro H, Ziel JW, Ihara S, Wang Z, Sherwood DR. Integrin Acts Upstream of Netrin Signaling to Regulate Formation of the Anchor Cell's Invasive

Membrane in C. elegans. Dev Cell [Internet]. 2009;17(2):187–98. Available from: http://dx.doi.org/10.1016/j.devcel.2009.06.006

18. Hagedorn EJ, Kelley LC, Naegeli KM, Wang Z, Chi Q, Sherwood DR. ADF/cofilin promotes invadopodial membrane recycling during cell invasion in vivo. J Cell Biol. 2014;204(7):1209–18.

19. Morrissey MA, Jayadev R, Miley GR, Blebea CA, Chi Q, Ihara S, et al. SPARC Promotes Cell Invasion In Vivo by Decreasing Type IV Collagen Levels in the Basement Membrane. PLoS Genet. 2016;12(2).

20. Hagedorn EJ, Ziel JW, Morrissey MA, Linden LM, Wang Z, Chi Q, et al. The netrin receptor DCC focuses invadopodia-driven basement membrane transmigration in vivo. J Cell Biol. 2013;201(6):903–13.

21. Kelley LC, Chi Q, Cáceres R, Hastie E, Schindler AJ, Matus DQ, et al. Adaptive F-actin polymerization and localized ATP production drive basement membrane invasion in the absence of MMPs. Dev Cell. 2019;48(3):313–28.

22. Medwig-Kinney TN, Smith JJ, Palmisano NJ, Tank S, Zhang W, Matus DQ. A developmental gene regulatory network for C. elegans anchor cell invasion. Development [Internet]. 2020 Jan 1;147(1):dev185850. Available from: http://dev.biologists.org/content/147/1/dev185850.abstract

23. Kohrman AQ, Matus DQ. Divide or Conquer: Cell Cycle Regulation of Invasive Behavior. Trends Cell Biol [Internet]. 2016;27(1):12–25. Available from: http://dx.doi.org/10.1016/j.tcb.2016.08.003

24. Matus DQ, Lohmer LL, Kelley LC, Schindler AJ, Kohrman AQ, Barkoulas M, et al. Invasive Cell Fate Requires G1 Cell-Cycle Arrest and Histone Deacetylase-

Mediated Changes in Gene Expression. Dev Cell [Internet]. 2015;35(2):162–74. Available from: http://dx.doi.org/10.1016/j.devcel.2015.10.002

25. Brand M, Nakka K, Zhu J, Dilworth FJ. Polycomb/Trithorax Antagonism: Cellular Memory in Stem Cell Fate and Function. Cell Stem Cell [Internet]. 2019;24(4):518–33. Available from: https://doi.org/10.1016/j.stem.2019.03.005

26. Simon JA, Tamkun JW. Programming off and on states in chromatin: Mechanisms of Polycomb and trithorax group complexes. Curr Opin Genet Dev. 2002;12(2):210–8.

27. Kadoch C, Williams RT, Calarco JP, Miller EL, Weber CM, Braun SMG, et al. Dynamics of BAF – Polycomb complex opposition on heterochromatin in normal and oncogenic states. Nat Publ Gr [Internet]. 2016;49(2):213–22. Available from: http://dx.doi.org/10.1038/ng.3734

28. Friman ET, Deluz C, Meireles-Filho ACA, Govindan S, Gardeux V, Deplancke B, et al. Dynamic regulation of chromatin accessibility by pluripotency transcription factors across the cell cycle. bioRxiv. 2019;1–28.

29. Ma Y, McKay DJ, Buttitta L. Changes in chromatin accessibility ensure robust cell cycle exit in terminally differentiated cells. PLoS Biol. 2019;17(9):1–29.

30. Bai J, Mei P, Zhang C, Chen F, Li C, Pan Z, et al. BRG1 Is a Prognostic Marker and Potential Therapeutic Target in Human Breast Cancer. PLoS One. 2013;8(3):1–9.

31. Kadoch C, Hargreaves DC, Hodges C, Elias L, Ho L, Ranish J, et al. a n a ly s i s Proteomic and bioinformatic analysis of mammalian SWI / SNF complexes identifies extensive roles in human malignancy. Nat Publ Gr [Internet].

2013;45(6):592–601. Available from: http://dx.doi.org/10.1038/ng.2628

32. Kaufmann B, Wang B, Zhong S, Laschinger M, Patil P, Lu M, et al. BRG1 promotes hepatocarcinogenesis by regulating proliferation and invasiveness. PLoS One. 2017;12(7):1–14.

33. Bögershausen N, Wollnik B. Mutational Landscapes and Phenotypic Spectrum of SWI/SNF-Related Intellectual Disability Disorders. Front Mol Neurosci. 2018;11(August):1–18.

34. van der Vaart A, Godfrey M, Portegijs V, van den Heuvel S. Dose-dependent functions of SWI/SNF BAF in permitting and inhibiting cell proliferation in vivo. Sci Adv. 2020;6(21).

35. Adikes RC, Kohrman AQ, Martinez MAQ, Palmisano NJ, Smith JJ, Medwig-Kinney TN, et al. Visualizing the metazoan proliferation-quiescence decision in vivo. Elife. 2020;9:1–74.

36. Rual JF, Ceron J, Koreth J, Hao T, Nicot AS, Hirozane-Kishikawa T, et al. Toward improving Caenorhabditis elegans phenome mapping with an ORFeome-based RNAi library. Genome Res. 2004;14(10 B):2162–8.

37. Kamath RS, Ahringer J. Genome-wide RNAi screening in Caenorhabditis elegans. Methods. 2003;30(4):313–21.

38. Matus DQ, Li X-Y, Durbin S, Agarwal D, Chi Q, Weiss SJ, et al. In vivo identification of regulators of cell invasion across basement membranes. Sci Signal [Internet]. 2010;3(120):ra35. Available from: http://www.pubmedcentral.nih.gov/articlerender.fcgi?artid=3917318&tool=pmcentrez&rendertype=abstract

39. W W. The SWI / SNF Family of ATP-Dependent Chromatin Remodelers□: Similar Mechanisms for Diver Function. In: Workman JL, editor. Protein Complexes that Modify Chromatin. Springer-Verlag Berling Heidelberg; 2003. p. 144–65.

40. Sawa H, Kouike H, Okano H. Components of the SWI/SNF complex are required for asymmetric cell division in C. elegans. Mol Cell. 2000;6(3):617–24.

41. Cui M, Fay DS, Han M. Lin-35/Rb cooperates with the SWI/SNF complex to control Caenorhabditis elegans larval development. Genetics. 2004;167(3):1177–85.

42. Large EE, Mathies LD. Caenorhabditis elegans SWI/SNF subunits control sequential developmental stages in the somatic gonad. G3 (Bethesda) [Internet]. 2014;4(3):471–83. Available from: http://www.pubmedcentral.nih.gov/articlerender.fcgi?artid=3962486&tool=pmcentrez&rendertype=abstract

43. Ertl I, Porta-De-La-Riva M, Gómez-Orte E, Rubio-Peña K, Corrales D, Cornes E, et al. Functional interplay of two paralogs encoding SWI/SNF chromatin-remodeling accessory subunits during Caenorhabditis elegans development. Genetics. 2016;202(3):961–75.

44. Cenik BK, Shilatifard A. COMPASS and SWI/SNF complexes in development and disease. Nat Rev Genet [Internet]. 2021;22(1):38–58. Available from: http://dx.doi.org/10.1038/s41576-020-0278-0

45. Kadoch C, Crabtree GR. Mammalian SWI/SNF chromatin remodeling complexes and cancer: Mechanistic insights gained from human genomics. Sci Adv [Internet]. 2015;1(5):e1500447–e1500447. Available from:

http://advances.sciencemag.org/cgi/doi/10.1126/sciadv.1500447

46. Nickerson JA, Wu Q, Imbalzano AN. Mammalian SWI/SNF enzymes and the epigenetics of tumor cell metabolic reprogramming. Front Oncol. 2017;7(APR):1–9.

47. Mittal P, Roberts CWM. The SWI/SNF complex in cancer — biology, biomarkers and therapy. Nat Rev Clin Oncol [Internet]. 2020;17(7):435–48. Available from: http://dx.doi.org/10.1038/s41571-020-0357-3

48. Ruijtenberg S, Van Den Heuvel S. G1/S Inhibitors and the SWI/SNF Complex Control Cell-Cycle Exit during Muscle Differentiation. Cell [Internet]. 2015;162(2):300–13. Available from: http://dx.doi.org/10.1016/j.cell.2015.06.013

49. Muchardt C, Yaniv M. When the SWI/SNF complex remodels...the cell cycle. Oncogene. 2001;20(24):3067–75.

50. Nagl NG, Zweitzig DR, Thimmapaya B, Beck GR, Moran E. The c-myc gene is a direct target of mammalian SWI/SNF-related complexes during differentiation-associated cell cycle arrest. Cancer Res. 2006;66(3):1289–93.

51. Moshkin YM, Mohrmann L, van Ijcken WFJ, Verrijzer CP. Functional Differentiation of SWI/SNF Remodelers in Transcription and Cell Cycle Control. Mol Cell Biol [Internet]. 2007;27(2):651–61. Available from: http://mcb.asm.org/cgi/doi/10.1128/MCB.01257-06

52. Son EY, Crabtree GR. The role of BAF (mSWI/SNF) complexes in mammalian neural development. Am J Med Genet C Semin Med Genet. 2014;(650).

53. Kuzmanov A, Karina EI, Kirienko N V., Fay DS. The Conserved PBAF Nucleosome-Remodeling Complex Mediates the Response to Stress in

Caenorhabditis elegans. Mol Cell Biol. 2014;34(6):1121–35.

54. Mathies LD, Blackwell GG, Austin MK, Edwards AC, Riley BP, Davies AG, et al. SWI/SNF chromatin remodeling regulates alcohol response behaviors in Caenorhabditis elegans and is associated with alcohol dependence in humans. Proc Natl Acad Sci U S A [Internet]. 2015;112(10):3032–7. Available from: /pmc/articles/PMC4364201/?report=abstract

55. Hayes GD, Riedel CG, Ruvkun G. The Caenorhabditis elegans somi-1 zinc finger protein and SWI/SNF promote regulation of development by the mir-84 microRNA. Genes Dev. 2011;25(19):2079–92.

56. Shibata Y, Uchida M, Takeshita H, Nishiwaki K, Sawa H. Multiple functions of PBRM-1/Polybromo- and LET-526/Osa-containing chromatin remodeling complexes in C. Elegans development. Dev Biol [Internet]. 2012;361(2):349–57. Available from: http://dx.doi.org/10.1016/j.ydbio.2011.10.035

57. Weinberg P, Flames N, Sawa H, Garriga G, Hobert O. The SWI/SNF chromatin remodeling complex selectively affects multiple aspects of serotonergic neuron differentiation. Genetics. 2013;194(1):189–98.

58. Riedel CG, Dowen RH, Lourenco GF, Natalia V, Heimbucher T, West JA, et al. DAF-16/FOXO employs the chromatin remodeller SWI/SNF to promote stress resistance and longevity. 2013;15(5):491–501.

59. Kipreos ET, van den Heuvel S. Developmental Control of the Cell Cycle: Insights from Caenorhabditis elegans. Genetics. 2019;211(3):797–829.

60. Sturm Á, Saskoï É, Tibor K, Weinhardt N, Vellai T. Highly efficient RNAi and Cas9-based auto-cloning systems for C. Elegans research. Nucleic Acids Res.

2018;46(17):1–13.

61. Dickinson DJ, Goldstein B. CRISPR-based methods for caenorhabditis elegans genome engineering. Genetics. 2016;202(3):885–901.

62. Rago F, DiMare MT, Elliott GN, Ruddy DA, Sovath S, Kerr G, et al. Degron mediated BRM/SMARCA2 depletion uncovers novel combination partners for treatment of BRG1/SMARCA4-mutant cancers. Biochem Biophys Res Commun [Internet]. 2019;508(1):109–16. Available from: https://doi.org/10.1016/j.bbrc.2018.09.009

63. Wang S, Tang NH, Lara-Gonzalez P, Zhao Z, Cheerambathur DK, Prevo B, et al. A toolkit for GFP-mediated tissue-specific protein degradation in C. elegans . Development. 2017;144(14):2694–701.

64. Ziel JW, Matus DQ, Sherwood DR. An expression screen for RhoGEF genes involved in C. elegans gonadogenesis. Gene Expr Patterns [Internet]. 2009;9(6):397–403. Available from: http://www.nature.com/doifinder/10.1038/jid.2014.371

65. Rimann I, Hajnal A. Regulation of anchor cell invasion and uterine cell fates by the egl-43 Evi-1 proto-oncogene in Caenorhabditis elegans. Dev Biol. 2007;308(1):187–95.

66. Deng T, Stempor P, Appert A, Daube M, Ahringer J, Hajnal A, et al. The caenorhabditis elegans homolog of the evi1 proto-oncogene, egl-43, coordinates G1 cell cycle arrest with pro-invasive gene expression during anchor cell invasion. PLoS Genet [Internet]. 2020;16(3). Available from: http://dx.doi.org/10.1371/journal.pgen.1008470

67. Spencer SL, Cappell SD, Tsai F, Overton KW, Wang L, Meyer T. The Proliferation-Quiescence Decision Is Controlled by a Bifurcation in CDK2 Activity at Mitotic Exit. 2013;155(2):369–83.

68. Cao Y, Cairns BR, Kornberg RD, Laurent BC. Sfh1p, a component of a novel chromatin-remodeling complex, is required for cell cycle progression. Mol Cell Biol. 1997;17(6):3323–34.

69. Angus-Hill ML, Schlichter A, Roberts D, Erdjument-Bromage H, Tempst P, Cairns BR. A Rsc3/Rsc30 zinc cluster dimer reveals novel roles for the chromatin remodeler RSC in gene expression and cell cycle control. Mol Cell. 2001;7(4):741–51.

70. Zhang L, Ward JD, Cheng Z, Dernburg AF. The auxin-inducible degradation (AID) system enables versatile conditional protein depletion in C. elegans. Development [Internet]. 2015;142(24):4374–84. Available from: http://dev.biologists.org/content/142/24/4374.abstract

71. Martinez MAQ, Kinney BA, Medwig-Kinney TN, Ashley G, Ragle JM, Johnson L, et al. Rapid degradation of C. elegans proteins at single-cell resolution with a synthetic auxin. G3 (Bethesda). 2020;10(January):267–80.

72. Wang L, Shen W, Lei S, Matus D, Sherwood D, Wang Z. MIG-10 (Lamellipodin) stabilizes invading cell adhesion to basement membrane and is a negative transcriptional target of EGL-43 in C. elegans. Biochem Biophys Res Commun [Internet]. 2014;452(3):328–33. Available from: http://dx.doi.org/10.1016/j.bbrc.2014.08.049

73. Sherwood, DR., Plastino J. Invading , Leading and Navigating Cells in

Caenorhabditis elegans□: Insights into Cell Movement in Vivo. In: WormBook□: the online review of C elegans biology. 2018. p. 53–78.

74. Ribeiro-Silva C, Vermeulen W, Lans H. SWI/SNF: Complex complexes in genome stability and cancer. DNA Repair. 2019.

75. Lu P, Roberts CW. The SWI/SNF tumor suppressor complex. Nucleus [Internet]. 2013;4(5):374–8. Available from: http://www.tandfonline.com/doi/abs/10.4161/nucl.26654

76. Hargreaves DC, Crabtree GR. ATP-dependent chromatin remodeling: Genetics, genomics and mechanisms. Cell Res [Internet]. 2011;21(3):396–420. Available from: http://dx.doi.org/10.1038/cr.2011.32

77. Yang YF, Pan YH, Tian QH, Wu DC, Su SG. CBX1 Indicates Poor Outcomes and Exerts Oncogenic Activity in Hepatocellular Carcinoma. Transl Oncol [Internet]. 2018;11(5):1110–8. Available from: https://doi.org/10.1016/j.tranon.2018.07.002

78. Bracken AP, Brien GL, Verrijzer CP. Dangerous liaisons: interplay between SWI/SNF, NuRD, and Polycomb in chromatin regulation and cancer. Genes Dev [Internet]. 2019;1–24. Available from: http://genesdev.cshlp.org/lookup/doi/10.1101/gad.326066.119

79. Wang G, Tang J, Zhan W, Zhang R, Zhang M, Liao D, et al. CBX8 suppresses tumor metastasis via repressing snail in esophageal squamous cell carcinoma. Theranostics. 2017;7(14):3478–88.

80. Ma J, Zhan Y, Xu Z, Li Y, Luo A, Ding F, et al. ZEB1 induced miR-99b/let-7e/miR-125a cluster promotes invasion and metastasis in esophageal squamous cell carcinoma. Cancer Lett. 2017;398:37–45.

81. Zhou D.X., Zhou D., Zhan S.Q., Wang P., Qin K., Gan W. LXF. Inhibition of JMJD6 expression reduces the proliferation, migration and invasion of neuroglioma stem cells. Neoplasma. 2017;64(5).

82. Pickard A, Cichon AC, Barry A, Kieran D, Patel D, Hamilton P, et al. Inactivation of Rb in stromal fibroblasts promotes epithelial cell invasion. EMBO J [Internet]. 2012;31(14):3092–103. Available from: http://dx.doi.org/10.1038/emboj.2012.153

83. Gillison ML, Akagi K, Xiao W, Jiang B, Pickard RKL, Li J, et al. Human papillomavirus and the landscape of secondary genetic alterations in oral cancers. Genome Res. 2019;29(1):1–17.

84. Bondy-Chorney E, Baldwin RM, Didillon A, Chabot B, Jasmin BJ, Côté J. RNA binding protein RALY promotes Protein Arginine Methyltransferase 1 alternatively spliced isoform v2 relative expression and metastatic potential in breast cancer cells. Int J Biochem Cell Biol [Internet]. 2017;91(March):124–35. Available from: http://dx.doi.org/10.1016/j.biocel.2017.07.008

85. Zhong S, Yan H, Chen Z, Li Y, Shen Y, Wang Y, et al. Overexpression of TAF1L promotes cell proliferation, migration and invasion in esophageal squamous cell carcinoma. J Cancer. 2019;10(4):979–89.

86. Yang L, Zeng W, Sun H, Huang F, Yang C, Cai X, et al. Bioinformatical Analysis of Gene Expression Omnibus Database Associates TAF7/CCNB1, TAF7/CCNA2, and GTF2E2/CDC20 Pathways with Glioblastoma Development and Prognosis. World Neurosurg [Internet]. 2020;138:e492–514. Available from: https://doi.org/10.1016/j.wneu.2020.02.159

87. Herpel E, Rieker RJ, Dienemann H, Muley T, Meister M, Hartmann A, et al.

SMARCA4 and SMARCA2 deficiency in non–small cell lung cancer: immunohistochemical survey of 316 consecutive specimens. Ann Diagn Pathol [Internet]. 2017;26:47–51. Available from: http://dx.doi.org/10.1016/j.anndiagpath.2016.10.006

88. Shibata Y, Uchida M, Takeshita H, Nishiwaki K, Sawa H. Multiple functions of PBRM-1/Polybromo- and LET-526/Osa-containing chromatin remodeling complexes in C. Elegans development. Dev Biol [Internet]. 2012;361(2):349–57. Available from: http://dx.doi.org/10.1016/j.ydbio.2011.10.035

89. Zhang Z, Wang F, Du C, Guo H, Ma L, Liu X, et al. BRM/SMARCA2 promotes the proliferation and chemoresistance of pancreatic cancer cells by targeting JAK2/STAT3 signaling. Cancer Lett [Internet]. 2017;402:213–24. Available from: http://dx.doi.org/10.1016/j.canlet.2017.05.006

90. Wu RC, Wang TL, Shih IM. The emerging roles of ARID1A in tumor suppression. Cancer Biol Ther. 2014;15(6):655–64.

91. Clapier CR, Iwasa J, Cairns BR, Peterson CL. Mechanisms of action and regulation of ATP-dependent chromatin-remodelling complexes. Nat Publ Gr [Internet]. 2017; Available from: http://dx.doi.org/10.1038/nrm.2017.26

92. Vries RGJ, Bezrookove V, Zuijderduijn LMP, Kia SK, Houweling A, Oruetxebarria I, et al. Cancer-associated mutations in chromatin remodeler hSNF5 promote chromosomal instability by compromising the mitotic checkpoint. Genes Dev. 2005;19(6):665–70.

93. Kadoch C, Copeland RA, Keilhack H. PRC2 and SWI/SNF Chromatin Remodeling Complexes in Health and Disease. Biochemistry. 2016;55(11):1600–

14.

94. Shain AH, Pollack JR. The Spectrum of SWI/SNF Mutations, Ubiquitous in Human Cancers. PLoS One. 2013;8(1).

95. Fernando TM, Piskol R, Bainer R, Sokol ES, Trabucco SE, Zhang Q, et al. Functional characterization of SMARCA4 variants identified by targeted exome-sequencing of 131,668 cancer patients. Nat Commun [Internet]. 2020;11(1):1–13. Available from: http://dx.doi.org/10.1038/s41467-020-19402-8

96. Medina PP, Romero OA, Kohno T, Montuenga LM, Pio R, Yokota J, et al. Frequent BRG1/SMARCA4-Inactivating mutations in human lung cancer cell lines. Hum Mutat. 2008;29(5):617–22.

97. Network TCGAR. Corrigendum: Comprehensive molecular profiling of lung adenocarcinoma. Nature. 2014;514(7521):262.

98. Witkowski L, Carrot-Zhang J, Albrecht S, Fahiminiya S, Hamel N, Tomiak E, et al. Germline and somatic SMARCA4 mutations characterize small cell carcinoma of the ovary, hypercalcemic type. Nat Genet. 2014;46(5):438–43.

99. Dutta A, Sardiu M, Gogol M, Gilmore J, Zhang D, Florens L, et al. Composition and Function of Mutant Swi/Snf Complexes. Cell Rep [Internet]. 2017;18(9):2124–34. Available from: http://linkinghub.elsevier.com/retrieve/pii/S2211124717301158

100. Hoffman GR, Rahal R, Buxton F, Xiang K, McAllister G, Frias E, et al. Functional epigenetics approach identifies BRM/SMARCA2 as a critical synthetic lethal target in BRG1-deficient cancers. Proc Natl Acad Sci U S A. 2014;111(8):3128–33.

101. Sasaki M, Ogiwara H. Synthetic lethal therapy based on targeting the vulnerability

of SWI/SNF chromatin remodeling complex-deficient cancers. Cancer Sci. 2020;111(3):774–82.

102. Reisman DN, Sciarrotta J, Wang W, Funkhouser WK, Weissman BE. Loss of BRG1/BRM in human lung cancer cell lines and primary lung cancers: Correlation with poor prognosis. Cancer Res. 2003;63(3):560–6.

103. Marquez-Vilendrer SB, Rai SK, Gramling SJ, Lu L, Reisman DN. Loss of the SWI/SNF atpase subunits BRM and BRG1 drives lung cancer development. Oncoscience. 2016;3(11–12):322–36.

104. Sulston JE, Horvitz HR. Post-embryonic cell lineages of the nematode, Caenorhabditis elegans. Dev Biol. 1977;56(1):110–56.

105. Katsanos D, Barkoulas M. Tissue-specific transcription factor target identification in the Caenorhabditis elegans epidermis using targeted DamID. bioRxiv [Internet]. 2020; Available from: https://doi.org/10.1101/2020.12.17.423252

106. Morrissey MA, Keeley DP, Hagedorn EJ, McClatchey STH, Chi Q, Hall DH, et al. B-LINK: A Hemicentin, Plakin, and Integrin-Dependent Adhesion System that Links Tissues by Connecting Adjacent Basement Membranes. Dev Cell. 2014;31(3):319–31.

107. Simmer F, Tijsterman M, Parrish S, Koushika SP, Nonet ML, Fire A, et al. Loss of the putative RNA-directed RNA polymerase RRF-3 makes C. Elegans hypersensitive to RNAi. Curr Biol. 2002;12(15):1317–9.

108. Porta-de-la-Riva M, Fontrodona L, Villanueva A, Cerón J. Basic Caenorhabditis elegans methods: Synchronization and observation. J Vis Exp. 2012;(64):1–9.

109. Dickinson DJ, Ward JD, Reiner DJ, Goldstein B. Engineering the Caenorhabditis

elegans genome using Cas9-triggered homologous recombination. Nat Methods. 2013;10(10):1028–34.

110. Dickinson DJ, Goldstein B. CRISPR-based methods for caenorhabditis elegans genome engineering. Genetics. 2016;202(3):885–901.

111. Dickinson DJ, Pani AM, Heppert JK, Higgins CD, Goldstein B. Streamlined genome engineering with a self-excising drug selection cassette. Genetics. 2015;200(4):1035–49.

112. Grove C, Cain S, Chen WJ, Davis P, Harris T, Howe K, et al. Using WormBase, a genome biology resource for Caenorhabditis elegans and related nematodes. Methods Mol Biol. 2018;1757:399–470.

113. Sturm Á, Saskoi É, Tibor K, Weinhardt N, Vellai T. Highly efficient RNAi and Cas9-based auto-cloning systems for C. elegans research. Nucleic Acids Res. 2018;46(17):e105.

114. Conte Jr. D, T. Macneil L, J. M. Walhout A, C. Mello C. RNA Interference in Caenorhabditis Elegans. Current Protocol in Microbiology. 2015. 1–39 p.

115. Martinez M, Matus D. Auxin-mediated Protein Degradation in Caenorhabditis elegans. Bio-Protocol. 2020;10(8).

116. Schindelin J, Arganda-Carreras I, Frise E, Kaynig V, Longair M, Pietzsch T, et al. Fiji: An open-source platform for biological-image analysis. Nat Methods. 2012;9(7):676–82.

Figure 1

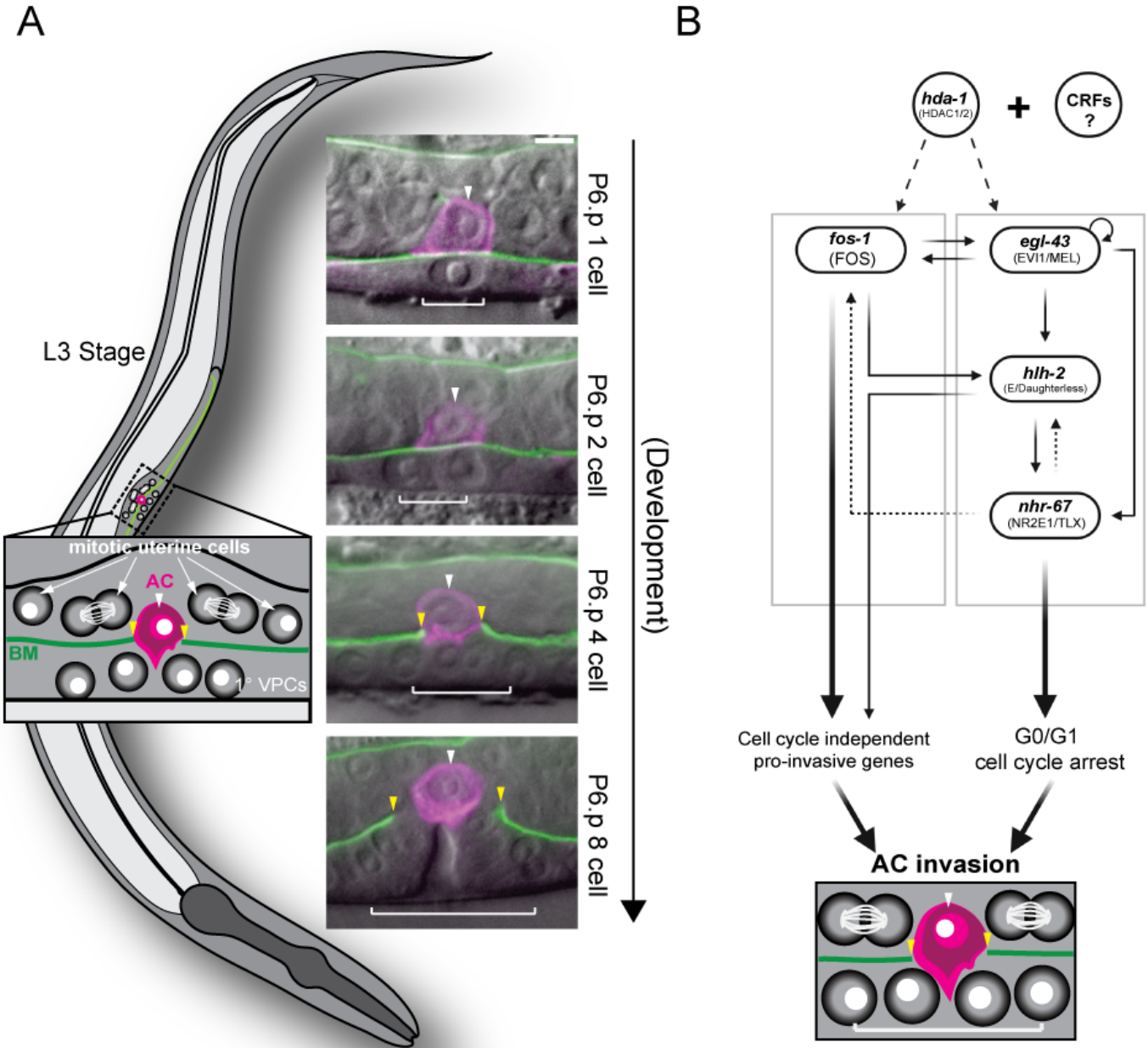
A
B
L3 Stage
mitotic uterine cells
AC
BM
1° VPCs
P6.p 1 cell
P6.p 2 cell
P6.p 4 cell
P6.p 8 cell
(Development)
hda-1
(HDAC1/2)
+
CRFs
?
fos-1
(FOS)
egl-43
(EVI1/MEL)
hlh-2
(E/Daughterless)
nhr-67
(NR2E1/TLX)
Cell cycle independent
pro-invasive genes
G0/G1
cell cycle arrest
AC invasion

Smith, et al. (2021)

Figure 2

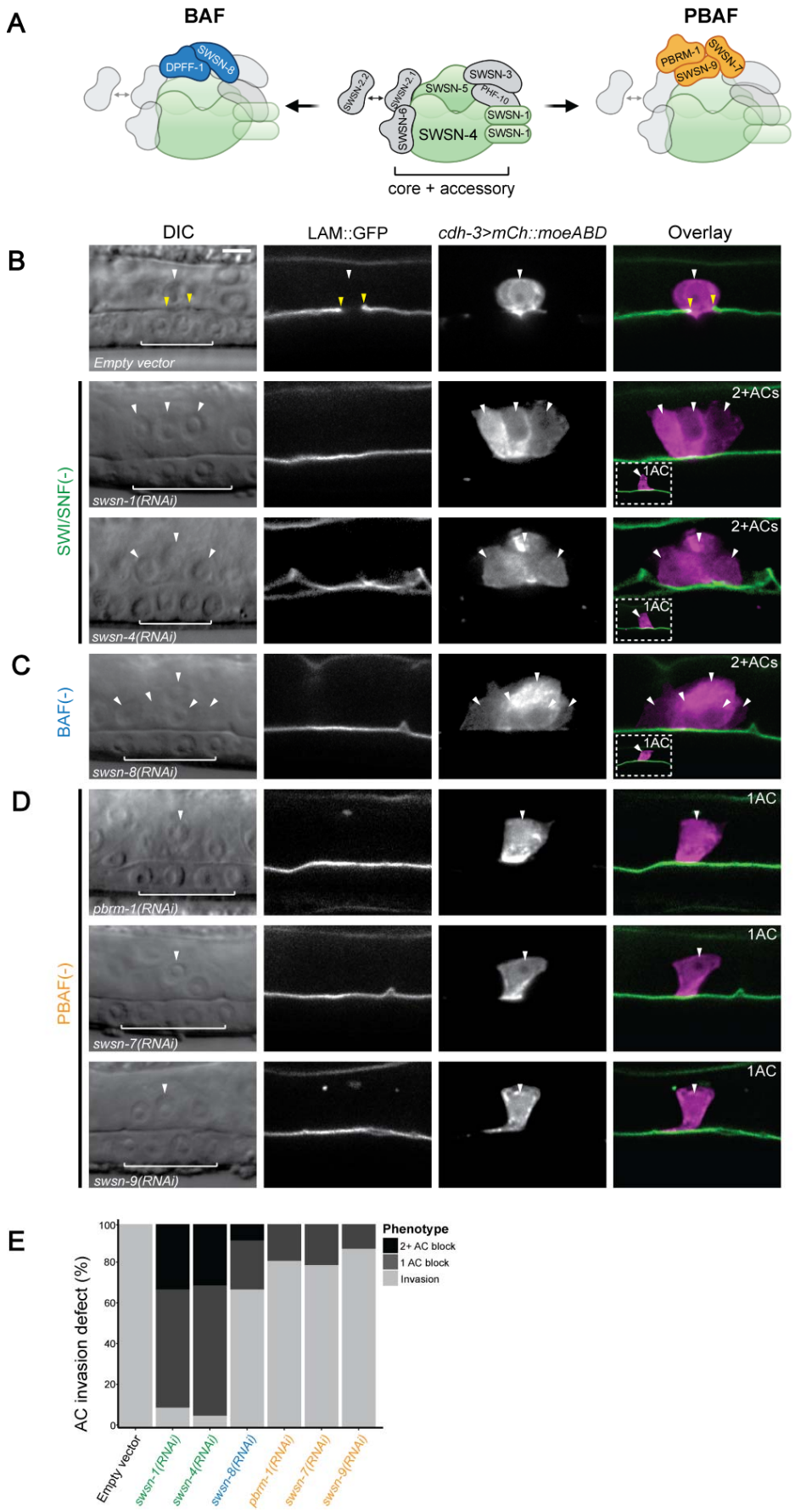

Figure 3

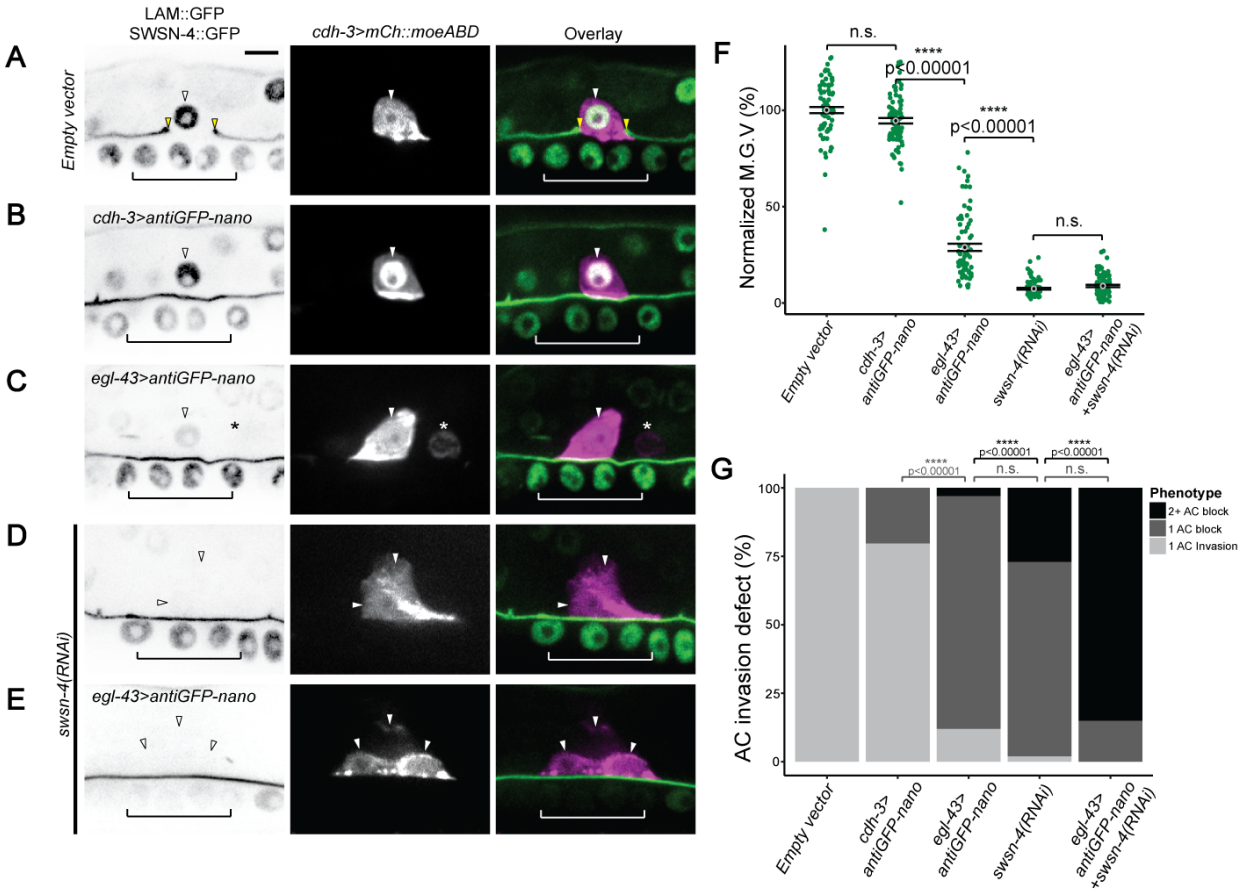
LAM::GFP
SWSN-4::GFP
cdh-3>mCh::moeABD
Overlay
A
Empty vector
B
cdh-3>antiGFP-nano
C
egl-43>antiGFP-nano
D
swsn-4(RNAi)
E
egl-43>antiGFP-nano
F
Normalized M.G.V (%)
n.s.
****
p<0.00001
****
p<0.00001
n.s.
Empty vector
cdh-3> antiGFP-nano
egl-43> antiGFP-nano
swsn-4(RNAi)
egl-43> antiGFP-nano +swsn-4(RNAi)
G
AC invasion defect (%)
Phenotype
2+ AC block
1 AC block
1 AC Invasion
****
p<0.00001
****
p<0.00001
n.s.
****
p<0.00001
n.s.

Figure 4

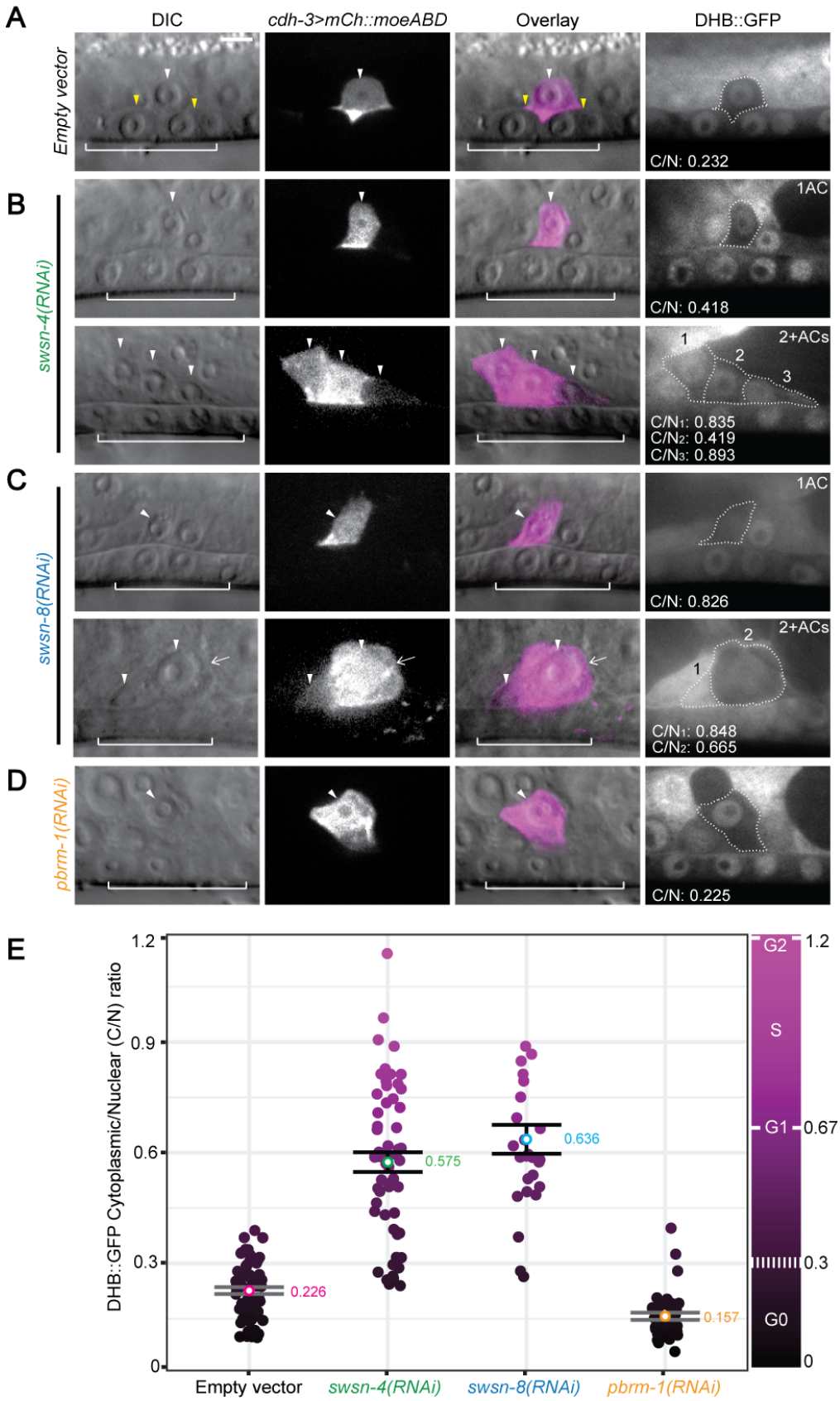
A
DIC
cdh-3>mCh::moeABD
Overlay
DHB::GFP
Empty vector
C/N: 0.232
B
swsn-4(RNAi)
1AC
C/N: 0.418
2+ACs
1
2
3
C/N1: 0.835
C/N2: 0.419
C/N3: 0.893
C
swsn-8(RNAi)
1AC
C/N: 0.826
2+ACs
2
1
C/N1: 0.848
C/N2: 0.665
D
pbrm-1(RNAi)
C/N: 0.225
E
DHB::GFP Cytoplasmic/Nuclear (C/N) ratio
1.2
0.9
0.6
0.3
0
0.226
0.575
0.636
0.157
Empty vector
swsn-4(RNAi)
swsn-8(RNAi)
pbrm-1(RNAi)
G2
S
G1
G0
1.2
0.67
0.3
0

Figure 5

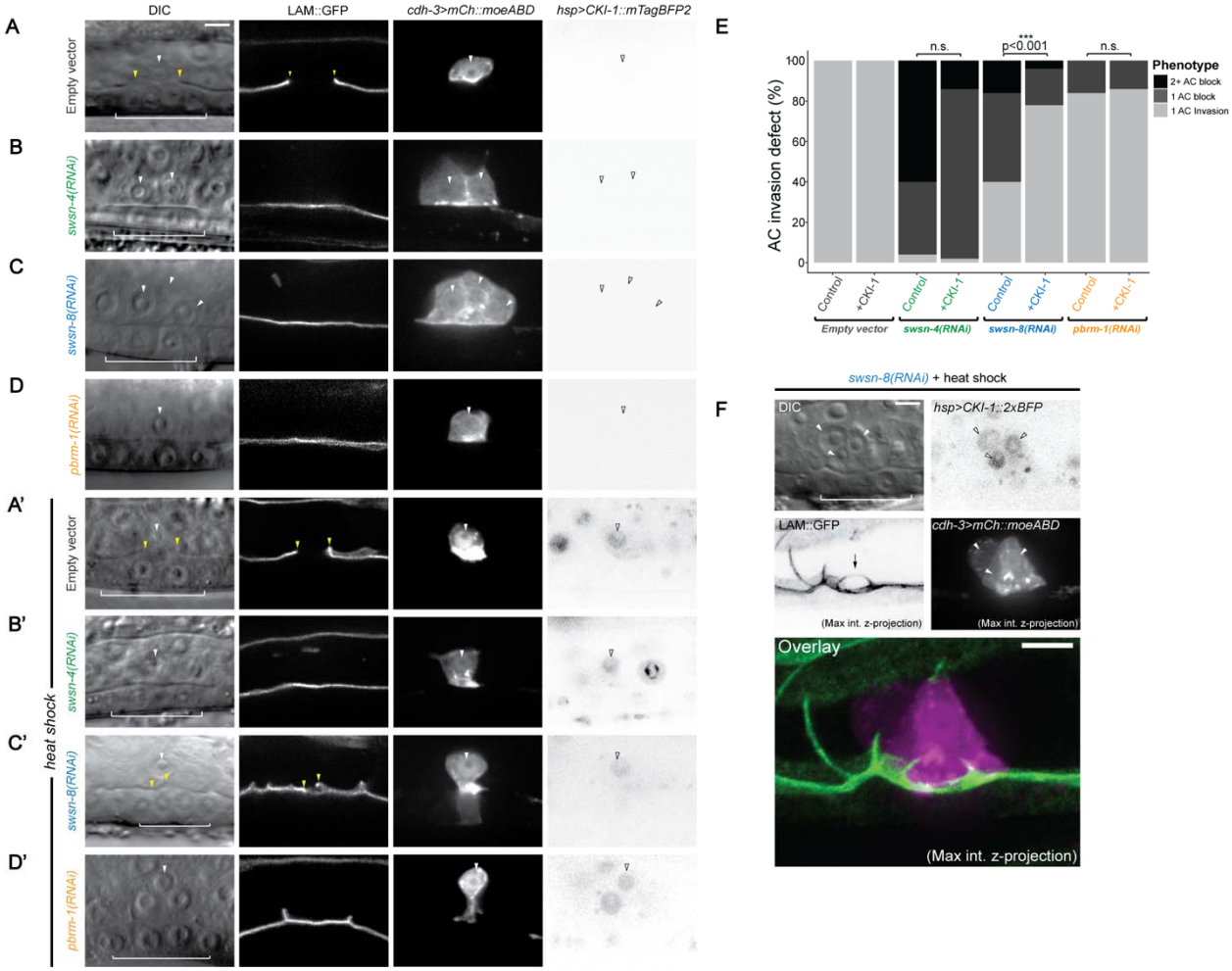
A
B
C
D
A'
B'
C'
D'
DIC
LAM::GFP
cdh-3>mCh::moeABD
hsp>CKI-1::mTagBFP2
Empty vector
swsn-4(RNAi)
swsn-8(RNAi)
pbrm-1(RNAi)
heat shock
E
AC invasion defect (%)
100
80
60
40
20
0
n.s.
***
p<0.001
n.s.
Phenotype
2+ AC block
1 AC block
1 AC Invasion
Control
+CKI-1
Empty vector
swsn-4(RNAi)
swsn-8(RNAi)
pbrm-1(RNAi)
F
swsn-8(RNAi) + heat shock
DIC
hsp>CKI-1::2xBFP
LAM::GFP
cdh-3>mCh::moeABD
(Max int. z-projection)
Overlay
(Max int. z-projection)

Figure 6

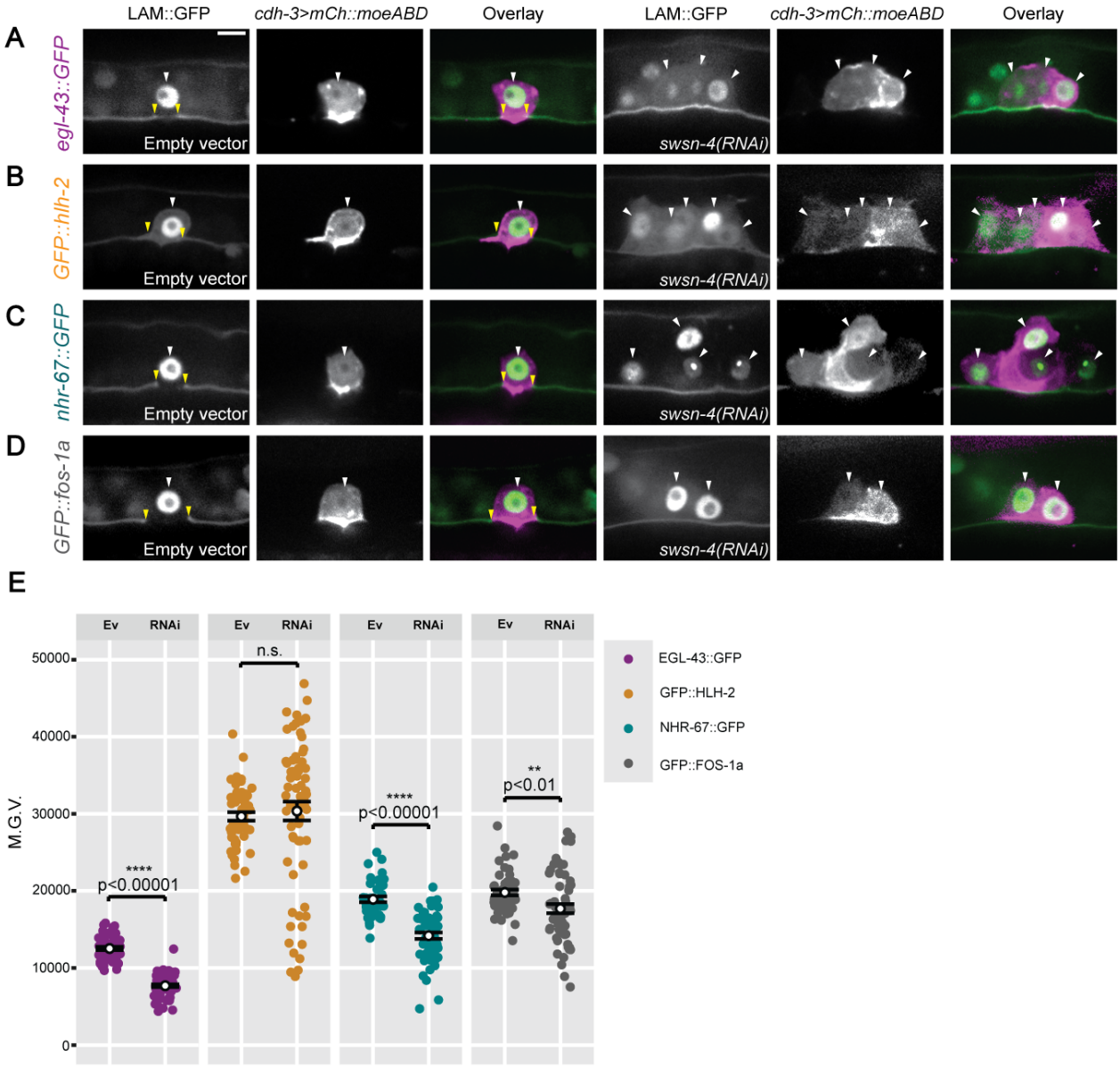
LAM::GFP
cdh-3>mCh::moeABD
Overlay
LAM::GFP
cdh-3>mCh::moeABD
Overlay
A
egl-43::GFP
Empty vector
swsn-4(RNAi)
B
GFP::hlh-2
Empty vector
swsn-4(RNAi)
C
nhr-67::GFP
Empty vector
swsn-4(RNAi)
D
GFP::fos-1a
Empty vector
swsn-4(RNAi)
E
Ev
RNAi
M.G.V.
50000
40000
30000
20000
10000
0
****
p<0.00001
n.s.
****
p<0.00001
**
p<0.01
EGL-43::GFP
GFP::HLH-2
NHR-67::GFP
GFP::FOS-1a

Figure 7

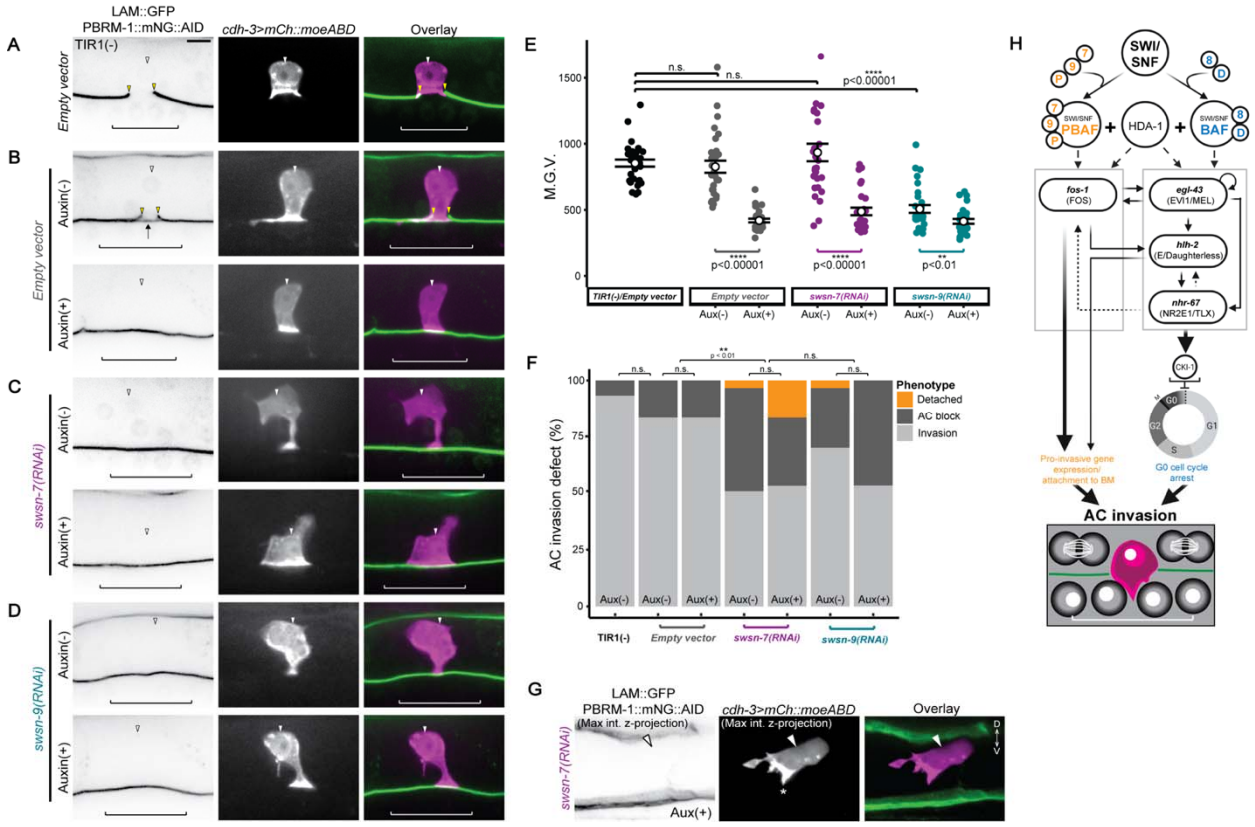
A
LAM::GFP
PBRM-1::mNG::AID
TIR1(-)
cdh-3>mCh::moeABD
Overlay
Empty vector
B
Auxin(-)
Auxin(+)
C
swsn-7(RNAi)
D
swsn-9(RNAi)
E
M.G.V.
n.s.
p<0.00001
p<0.01
TIR1(-)/Empty vector
Empty vector
swsn-7(RNAi)
swsn-9(RNAi)
Aux(-)
Aux(+)
F
AC invasion defect (%)
Phenotype
Detached
AC block
Invasion
G
(Max int. z-projection)
H
SWI/SNF
PBAF
HDA-1
BAF
fos-1 (FOS)
egl-43 (EVI1/MEL)
hlh-2 (E/Daughterless)
nhr-67 (NR2E1/TLX)
CKI-1
G0
G1
S
G2
Pro-invasive gene expression/ attachment to BM
G0 cell cycle arrest
AC invasion